energies

MDPI

Review

Estimation of Petrophysical Parameters of Carbonates Based on Well Logs and Laboratory Measurements, a Review

Marek Stadtműller [1] and Jadwiga A. Jarzyna [2,*]

[1] Oil and Gas Institute-National Research Institute, ul. Lubicz 25A, 31-503 Krakow, Poland; stadtmuller@inig.pl
[2] Faculty of Geology Geophysics and Environmental Protection, AGH University of Krakow, al. Mickiewicza 30, 30-059 Krakow, Poland
* Correspondence: jarzyna@agh.edu.pl

Abstract: The purpose of this review paper is to show the possibilities of carbonate reservoir characterization using well logging and laboratory measurements. Attention was focused on standard and new methods of well logging acquisition and interpretation including laboratory experiments to show a part of the history of carbonate rock investigations as hydrocarbon or water reservoirs. Brief information on the geology, mineralogy and petrography of carbonate rocks was delivered. Reservoir properties, i.e., porosity (including fracturing), permeability, and saturation, were defined to emphasize the specific features of carbonates, such as fractures, and vugs. Examples of methodologies were selected from the commonly used laboratory techniques (thin sections examination, mercury and helium porosimetry, X-ray diffraction—XRD) combined with the standard well logs (bulk density—RHOB, neutron porosity—NPHI, sonic slowness—DT, and deep resistivity—Rd) to show the methods that have been used since the very beginning of the scientific and engineering studies of carbonates. Novelty in well logging, i.e., resistivity and acoustic imaging, nuclear magnetic resonance–NMR, dipole shear sonic imaging–DSI, and a spectral neutron-gamma log-geochemical device–GLT combined with modern laboratory investigations (NMR laboratory experiments, scanning *electron* microscopy SEM), showed how continuous information on mineral composition, porosity and saturation could be obtained and juxtaposed with very detailed laboratory data. Computed X-ray tomography (CT) enabling the 2D and 3D analyses of pores and fractures was presented as a quantitative methodology, effective in pore space characterization, revealing rock filtration abilities. Deep learning and artificial intelligence were used for joining various types of data. It was shown that thanks to new computational technologies original data from very small samples (micro scale), extensively describing the flow ability of the reservoir, could be extended to mezzo scale (core samples) and macro scale (well log images). Selected examples from the published papers illustrated the review. References cited in the text, together with the issues included in them, were the rich source of the practical knowledge processed These were checked by the authors and could be used in other projects.

Keywords: carbonate reservoirs; petrophysical parameters; well logging; laboratory investigations; a review

Citation: Stadtműller, M.; Jarzyna, J.A. Estimation of Petrophysical Parameters of Carbonates Based on Well Logs and Laboratory Measurements, a Review. *Energies* **2023**, *16*, 4215. https://doi.org/10.3390/en16104215

Academic Editor: Rouhi Farajzadeh

Received: 22 February 2023
Revised: 4 May 2023
Accepted: 17 May 2023
Published: 20 May 2023

1. Introduction

For many years, the job of petroleum geologists and petrophysicists was, and still is, the recognition and characterization of geological formations, which are prospective for hydrocarbons (HC) [1–3]. Now, reservoir rock characterization is also important for geothermal recognition and prospection for hot underground geothermal waters, drinking and mineral waters, and hot dry rocks (HDR). Carbon sequestration, as a process of capturing and storing carbon dioxide in the underground space, also utilizes the reservoir properties of rocks.

The most important and prioritized parameters of reservoir rocks, inextricably linked to each other, are porosity and permeability. The general porosity definition includes

intergranular porosity together with fractures, fissures and vugs comprising all voids in the reservoir rock filled with media [1–6]. An integrated approach to fractured porous rocks was influenced, among other reasons, by intensive investigations of multiphase fluid flow in reservoirs [7], and utilizing the results in HC and water prospection. From a geological and petrophysical point of view, the most important definitions are those related to the origin of rocks and post-generated processes, taking place when rocks were established. Carbonate rocks comprise two main lithology types: limestone, built mainly of calcite (calcium carbonate); and dolomite, built of calcium and magnesium carbonate (dolomite mineral). In carbonate reservoirs, vugs (pores larger than grains), intergranular (between grains), and intragranular or cellular (within grains) porosity can be found together with moldic, and chalky porosity. Important parts of the total porosity of carbonates include fractures, fissures and cracks of different origin. Dolomitization, fracturing, dissolution, and recrystallization, as the results of diagenesis, are processes that create effective secondary porosity. On the other hand, cementation, another type of diagenesis, generally reduces porosity and permeability. It is important to remember that HC production from carbonates is almost twice the amount of hydrocarbons from clastic reservoirs and more than 50% of the world reserves [8,9] (Figure 1).

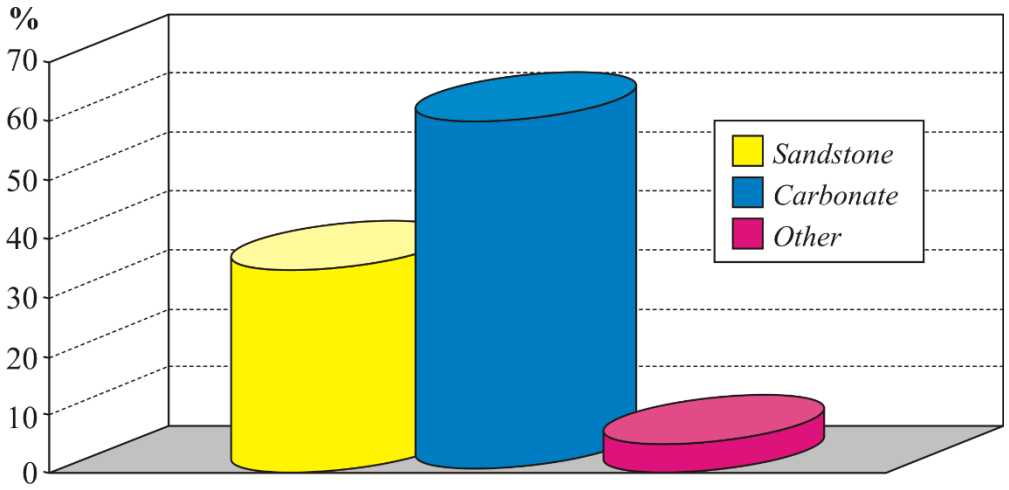

Figure 1. Production from sedimentary reservoirs (modified after [9]).

Following the title, the authors discussed the methodologies used for petrophysical characterization of carbonates, remaining aware that many technologies, especially in well logging, have been designed, tested and primarily processed in clastic rocks. The authors would also like to underline that the discussed methodologies using older well logging methods and laboratory experiments were never divided according to level of usefulness, but were presented as more or less advantageous on the background of geological conditions of reservoirs.

The list of well logs, the outcomes of which were discussed in the presented review paper, encompassed caliper (CAL), different resistivity logs (LLD, LLS, MSFL, micrologs in electric imaging logs), bulk density (RHOB), acoustic/sonic slowness of compressional wave (DT), neutron porosity (NPHI), dipmeter SED, resistivity imaging (Formation Micro Imager FMI, X-tended Range Micro Imager XRMI), acoustic imaging (Ultrasonic Borehole Imager UBI, Circumferential Acoustic Sidewall/Scanning Tool CAST), nuclear magnetic resonance NMR (relaxation times T1 and T2), and dipole shear sonic imager DSI (velocities of compressional, shear and Stoneley waves). The outcomes of geochemical log GLT (volume or mass of elements building minerals and rocks) were discussed on the base of the results presented in the referenced articles. Dielectric log, photoelectric factor PEF, and multi-array resistivity device were only listed after authors of the selected references issues.

2. Selected Features of Carbonates

Carbonates all over the world are differentiated by geographical location, stratigraphic position, sedimentary environment, depth, influence of tectonic phenomena and other factors. Sedimentation in various environments, subsequent diagenesis, and deformation means that they are highly heterogeneous, and reveal different fabrics and structures. So, the multi-scale, and multi-methodology approach was suitable in carbonate studies from the very beginning. The results in the analyzed papers were always presented on the background of local geological conditions. Reservoir parameters were strictly connected with the structure, and texture of rocks, mineral composition, chemical interactions, and pressure. So, in the study, a short analysis of basic features of carbonates was included to make the identification of common factors easier, and to build a platform for comparison.

2.1. Information on Classification of Carbonates

The most widely used classifications of carbonates were presented by Folk [10,11], and Dunham [12]. Thirty years later, the limestone classification was revised by Wright [13]. One year earlier, Embry and Klovan [14] published the modified Dunham division.

The scheme by Folk [10,11] is based on the proportions between matrix (very fine-grained carbonate), and components of skeleton, i.e., transported and changed grains. Pure mud or micrite is at one end of the spectrum, at the other end one can see the clast-supported frameworks with no mud. Generally, Folk's carbonate classification encompasses the influence of sedimentation conditions (energy), and is mainly applied to thin sections.

Dunham scheme [12] is also based on texture and structure of carbonate rocks. It uses the following components: (i) muddy limestones and grainstones (having no mud), and other components in between of different volumes of carbonate mud, (ii) mudstones, wackestones or packstones, and (iii) boundstones with binding agents. This classification is more useful in cores and outcrops examination.

Embry and Klovan's classification [14] was an extension of Dunham's scheme. To Dunham's components, they added floatstone, rudstone, bafflestone, bindstone, and framestone. The mudstone and bafflestone components are allochems, not organically bound during deposition, in contrary to the rest of components.

Wright [13] proposed two categories of diagenetic textures: non-obliterative, almost totally composed of diagenetic cement, and obliterative, including limestones and dolomites, where the original fabric has been destroyed. He also included sub-categories based on the crystal size [13].

Perras and Diederichs [15] completed the geological classifications based on sedimentary features by geotechnical elements including mechanical properties. In their opinion, the micro-mechanical features of various types of carbonates influenced fractures propagation. Argillaceous component could stop the fracture propagation, while bedding planes of low tensile strength could work as fracture propagation ways. Perras and Diederichs [15] stated, that the nature of carbonates, and mudrocks had unique petrophysical and geotechnical characteristics, which could be important for applications in geological engineering.

Some unification of the nomenclature was published in 2016 by Lokier and Mariam Al Junaibi [16]. On the basis of statistical results of the specific project, authors tried to find a kind of guideline to improve the classification of carbonate lithology, make easier communication between researchers, and facilitate the development of more realistic models of carbonate rocks. The authors concluded that the Dunham system [12] modified by Embry and Klovan [14] was popular and widely applied.

In the published literature, many local divisions of carbonate rocks related to the special sedimentation conditions can be found. As an example, the works of Wagner and Peryt [17] and Jaworowski and Mikołajewski [18] were cited to illustrate specific situation in the Main Dolomite, the most famous HC deposit in Poland.

In each cited paper, from which the discussed examples were taken, local classifications were also included, generally referred to aforementioned divisions.

2.2. Mineral Composition

Carbonate rocks make up 10–15% of sedimentary rocks. They are ideal reservoirs for HC and water, because of their often high porosity and permeability. They are soluble in slightly acid waters in contrary to hard sandstone reservoirs. According to a largely used definition, carbonates are rocks containing more than 50% carbonate minerals [19].

The dominant minerals are calcite and dolomite with admixture of anhydrite and siliciclastic components. A composite scheme for classifying carbonates is presented in Figure 2. Relative amounts of calcite and dolomite, as the main components, are presented as calcite/dolomite ratio or dolomite percentage in carbonate. Four subdivisions are presented as: limestone, dolomitic limestone, calcareous dolomite and dolomite [19]. Primary textures are deformed by sedimentary conditions, which influence porosity and permeability.

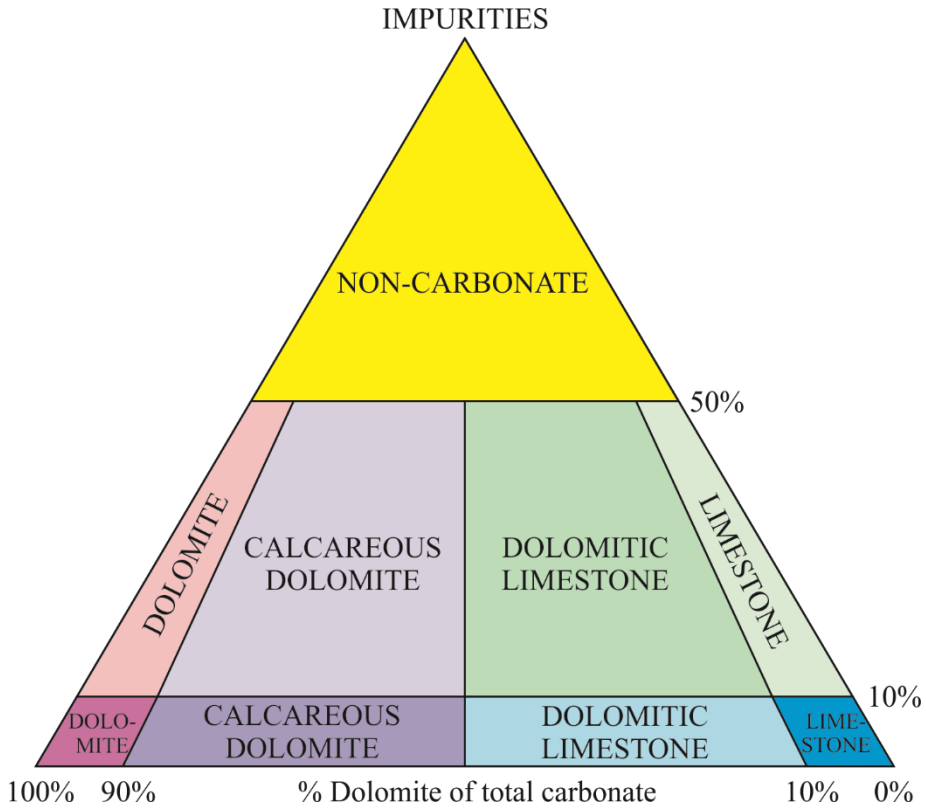

Figure 2. Composite scheme for classifying carbonates (modified after [19]).

2.3. Porosity

Reservoir rock porosity varies in a large range. In carbonates, it greatly exceeds the theoretical maximum porosity, when the rock is highly fractured or reveals vuggy porosity [1,4,20].

The average permeability of reservoir rocks (among other carbonates) is in the range 5–1000 mD. A dense limestone has a permeability of $\leq$5 mD. The permeability of reservoirs is roughly classified as: fair 1–10 mD, good 10–100 mD, and very good 100–1000 mD [1,2].

Total porosity informs about the ability of reservoir to fluid storage. Primary porosity means pore space built in a sediment during deposition/sedimentation. Secondary porosity means a post depositional porosity. This type of porosity, important for carbonates, results from groundwater dissolution, recrystallization and fracturing.

Effective porosity, widely used in petrophysics, comprises the interconnected pore volume available to free fluids [2,20–22].

Fracture porosity means openings nascent during the breaking or shattering of a rock. All rock types are affected by fracturing, and the mineral composition of the rock is a main determinant of how brittle the rock can be, and how many fractures will occur. Naturally,

fractured reservoirs are heterogeneous in comparison to not fractured ones, and it is visible in a matrix, built of original rock, divided into parts by fracture system. The matrix and the fracture systems are characterized by their own porosity and permeability, different from each other, so a naturally fractured reservoir can be treated as a double-porosity and double-permeability reservoir [6].

From a petrophysical point of view, regardless of rock lithology, two types of fractures are observed in rocks on the borehole wall: (i) natural (tectonically related) and (ii) induced (related to the drilling processes). Next to the two mentioned types of fractures, artificial hydraulic fractures and fissures, created by fluids injected into rock at pressures exceeding the strength of the rock, are considered. Hydraulic fracturing can tremendously increase the effective porosity and permeability of a formation [23]. The brittleness of a reservoir is an important parameter characterizing the hydraulic fracturing [24]. Brittle reservoirs, on the contrary to ductile ones, respond well to hydraulic fracturing [25]. Earlier, artificial acid fracturing was also utilized in carbonate reservoirs to enhance production and maximize recovery [26].

Vuggy porosity is a secondary porosity. It is a result of the dissolution of soluble parts of rock, and can also be a result of the enlargement of pores or fractures. Vugs are macroscopically or microscopically observed, because they are larger than adjacent grains or crystals. Permeability is significantly affected by vuggy porosity. Additionally, pressure drop and recovery factor in the reservoir are influenced by it [27]. Touching vugs, observed when fracturing decrease, are important because they can increase production [28]. Gomaa and co-authors added two definitions of vugs: (i) pores of throats of diameters >5 microns, observed in the mercury injection capillary pressure experiments, and (ii) pores, filled with water or light oil, larger than approximately 50 microns, observed in the NMR log outcomes [29].

The reason for the presence of moldic porosity, an important type of secondary porosity, is the dissolution of primary components of rocks, such as grains, shells, and rock fragments. In this type of porosity, the pore space shape is the same as the dissolved material [30]. Moldic pore size and packing, and moldic pore connectivity are variables controlling the relationship between permeability and porosity [31].

Chalk porosity is treated separately. Chalk is a microporous rock built of very small particles (μm radius) from phytoplankton microorganisms. The rock has low permeability (below 10 mD) [32]. In [33], it was found that "newly deposited chalk has interparticle porosity between the sediment grains, and intraparticle porosity within shells of microfossils", but the final value depends on depth, continuous burial, load of the increasing overburden, type of pore water and sediment relationships, presence of stylolites, and pressure dissolution. This special definition of chalk porosity is related to the North Sea HC deposits, especially Ekofisk formation [34].

In Figure 3, there is an illustration of selected types of porosity.

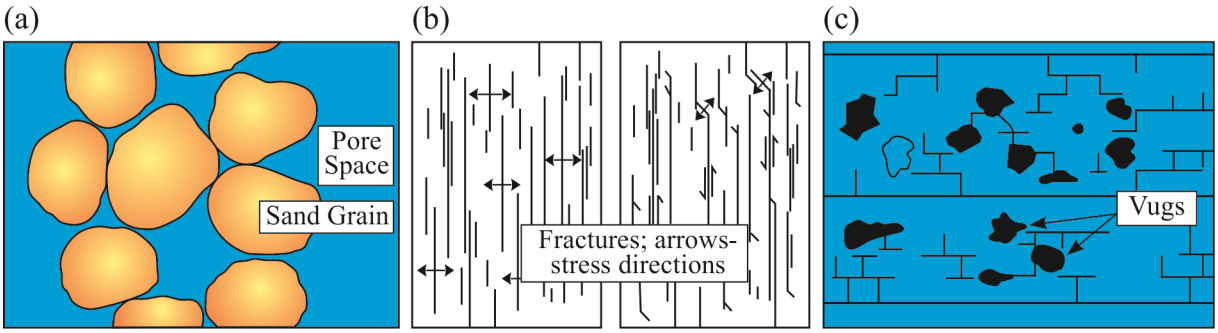

Figure 3. Various types of porosity; (**a**) primary, intergranular; (**b**) secondary, fractures; (**c**) secondary, vugs.

2.4. Factors Controlling Porosity and Permeability

Grain sorting, packing, compaction, cementation and crystallization are the main factors controlling rock reservoir properties. The following rule can be established for sorting—the better grains are sorted, the higher the total porosity. Packing depends on grain size, shape, and degree of compaction. Packing causes grain rearrangement, from open—cubic to the tightest or closed—rhombohedral type [35,36]. Compaction, i.e., the weight of the overlying sediments and pressure, squeezes mineral particles together into the tightest arrangement. Additionally, it removes water, and reduces the volume of the rock. So, finally there is observed decrease in porosity and permeability. Cementation is the process of lithification of the sediment. Calcite, silica and iron oxide are the important cementing agents. Cementation significantly reduces porosity and permeability.

Interconnected porosity (intergranular or intercrystalline porosity, interconnected vugs, or fractures) is an immanent feature of the permeable formations. A lack of interconnected pores, i.e., closed or frequently empty voids in the rock, does not contribute to permeability, because there is no flow through them [22]. Even if rocks are filled with hydrocarbons, HC could not be extracted due to pores isolation, and formed the residual oil saturation (ROS) (Figure 4). Limestones may exhibit very low permeability due to a lack of interconnected vugs, but naturally (or even hydraulically) fractured ones can show an increase in this parameter due to the interconnection of the isolated pores by the fractures. Pressure, type of fluids, and their viscosity are considered together as factors influencing permeability. The following rules are in common use: higher pressure allows a higher flow rate, and more viscous fluid causes greater difficulty in flowing through the rock.

Mutual relationships between permeability and saturation may be explained in the plot between relative permeability vs. saturation (water and hydrocarbons) [1,37] (Figure 4). The definition of the relative permeability is based on the amount of one type of fluid, that flows in the presence of other fluid/fluids. Volume of fluid, flowing together with the other one, is related to the volume that flows at the saturation of 100%, with all other factors unchanged [38]. Irreducible water saturation (Swirr) is defined as the value of water saturation when water flow is finished (Figure 4). When Sw (water saturation) increases, water flow starts to be observed, and Krw increases, because capillary pressure cannot keep water still in pore space. In this section of the plot (Figure 4), the relative permeability of oil to water (Kro) will continue to decrease, and the relative permeability of water to oil (Krw) will increase. Residual oil saturation (ROS) (Figure 4) is defined when water saturation will reach the value, at which the relative permeability of oil to water (Kro) is equal to 0. At ROS point, oil will no longer flow within the reservoir.

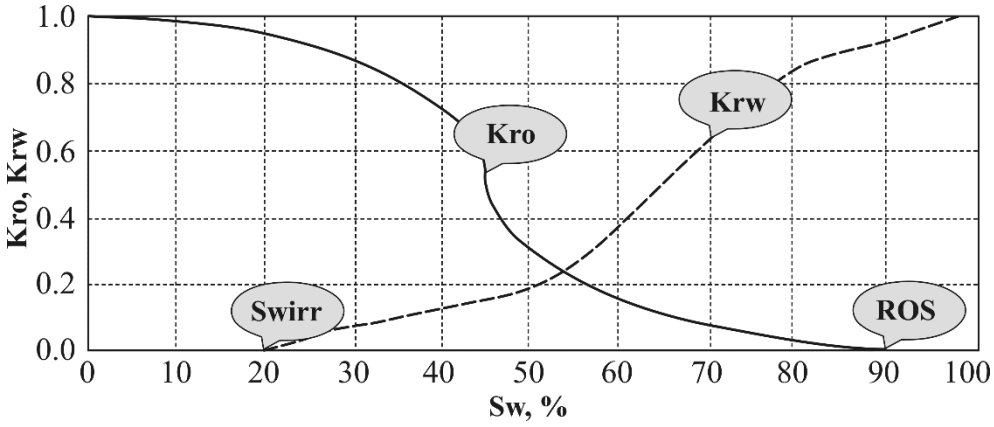

Figure 4. Relations between relative permeability and water saturation.

F. Jerry Lucia devoted several papers to geological and petrophysical features of carbonates [39–44]. He followed Archie's approach [45], and focused on spatial distribution of porosity, permeability, and saturation. He concluded that pore-size distribution was

related to rock fabric, which was a result of the sedimentary, geologic processes. We cite here his words, "to determine the relationships between rock fabric and petrophysical parameters, one must define and classify pore space as it exists today in terms of petrophysical properties" [41]. In his opinion, permeability and capillary parameters of the non-vuggy rocks could be described by particle size, sorting and interparticle porosity, and total porosity could be lowered by vuggy porosity. Lucia [41] used the Dunham's approach [12] to describe particle size, and sorting in limestones defining "packstone as grain dominated or mud dominated, depending on the presence or absence of intergrain pore space". He also included dolomite crystal size in dolostones description because, in his opinion, "larger dolomite crystal size improves petrophysical properties in mud-dominated fabrics". Lucia [41] emphasized that in the comprehensive interpretation of geological and petrophysical features of reservoir rocks, division into interparticle and vuggy porosity was important. Next, vuggy porosity was partitioned into separate vugs, communicated only through the interparticle pores, and vugs building a joint pore system. Thus, an interpreter must classify the carbonate into three types: interparticle, separate vug or touching vug, and determine the pore space in these classes. Lucia proposed changing the grain-supported and mud-supported classes to grain-dominated and mud-dominated types. In the mud-dominated type, spaces between the grains are made of mud, and grains form a supporting structure [41]. It is worth mentioning here that F. Jerry Lucia was the geological engineer in the Shell Oil Company, who promoted combining laboratory and well logging petrophysical measurements to obtain information from various sources.

A team of S.N. Ehrenberg, G.P. Eberli, M. Keramati and S.A. Moallemi, formed by HC prospecting practitioners and members of universities' scientific groups, presented porosity–permeability relationships in interlayered limestone–dolostone reservoirs [46]. On the base of data compiled from five platform successions (Figure 5), differentiated as regards geographical site, stratigraphy and depth, they showed the special features of interlayered limestones and dolostones [47–55]. Dividing the data on the base of burial depth into shallow, and deep buried platforms, they showed the differences in mineral composition and reservoir properties of limestones and dolostones in various sedimentary environments (Figure 5). They assumed that the data were so differentiated that recognized similarities would be representative of carbonates all over the world. Frequency histograms of porosity, plots of porosity vs. depth, and cross-plots permeability vs. porosity were used for formation characterization. The authors stated that limestones and dolostones at shallowly buried platforms revealed insignificant differences in average porosity. Data from these platforms showed higher average permeability for given porosity in dolostones compared to limestones. In contrary, the samples from deeply buried platforms limestones revealed much lower average porosity than dolostones. Little difference in average permeability was observed for a given porosity between limestones and dolostones. On the base of mineral composition (calcite, dolomite, and noncarbonate mineral volume) from different laboratory methods (XRD, bulk chemical analyses, thin sections), the authors defined the dolomite index (DI), equal to the ratio of dolomite to carbonate volume multiplied by 100. In all data sets, samples of DI ranging between 75 and 100% were included in the dolostone group. Samples with DI ranging between 0 and 25% grouped the wackestones and packstones. In these rocks, the mud matrix was partly replaced by dolomite. In the opinion of the cited authors, the index DI was an indicator of the process of dissolution of the remaining calcium carbonate in the partial dolomitization. In their conclusions, Ehrenberg et al. [46] confirmed the frequently expressed opinion, that dolostones preserved the porosity during burial cementation. Tight limestones built the barriers by chemical compaction, resulting in cementation in the burial processes. The authors emphasized the process of early dolomitization resulting in porosity preservation during burial. However, the deeply buried dolostones did not show higher permeability for given porosity than associated limestones. The relationship between permeability and porosity before the burial processes is similar for limestones and dolostones, but dolostones have bigger permeabilities. After burial, low-permeability limestones were strongly affected by diagenesis, causing a distinct

decrease in permeability. In high-permeability limestones, at the beginning, the decrease in permeability was similar, due to the presence of the more grain-supported textures, opposing the lowering of the permeability. As a result, the limestones and dolostones of significant permeability from the deeper sites have porosity vs. permeability relationships similar to those presented for other depths.

We described this paper in detail because the issues discussed by Ehrenberg's team explain the relations between sedimentary conditions and measured petrophysical parameters.

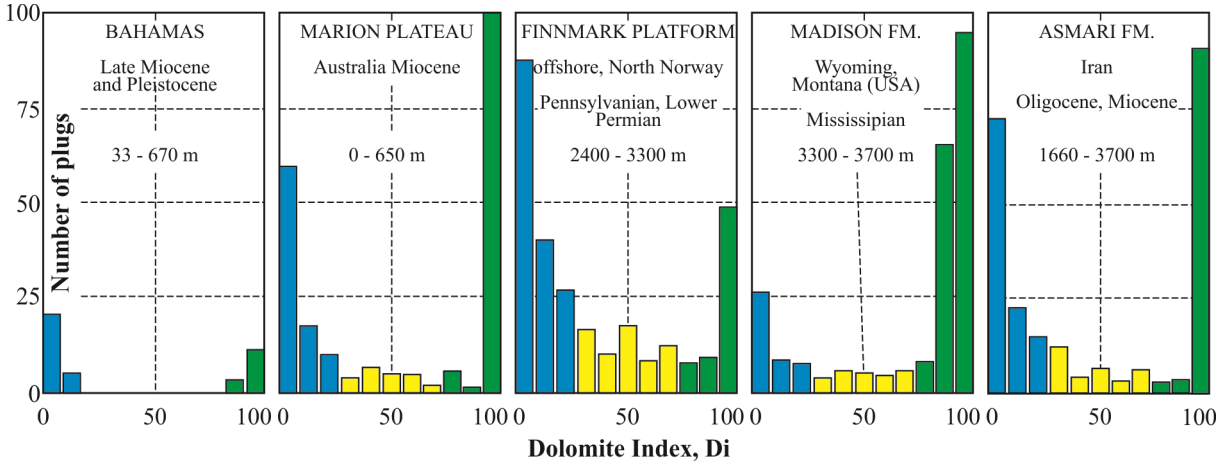

Figure 5. Proportion between limestone and dolostone samples in five data sets being the base for recognition of differences between reservoir properties of carbonates of various burial depth (two left are shallow platforms, three right are deep platforms) (after [46], modified). Colors are related only to Di range: $0 \leq Di \leq 25$—blue, $25 < Di \leq 75$—yellow, $75 < Di \leq 100$—green.

In the discussion about factors controlling the porosity and permeability of reservoirs, it is important to call once more the influence of mechanical status of an orogen on fractures and fluid flow [15]. The general structure of the reservoir and its environment is on the verge of mechanical failure [56]. Taking this into consideration, the bulk permeability of rock is influenced by changing stresses that are induced by the development of a HC reservoir in production. Permeability changes are related to dilatation, or compression of fractures, or faults, or new fractures in previously intact rock. Heffer [56] suggested that shear failure is a main factor controlling such changes.

3. Methods Used for Fracture Identification

In this section, several papers were discussed to illustrate how laboratory investigations and well logging measurements could be utilized in reservoir parameters recognition. The purpose of the review paper was to show different ways, used by the authors of publications, to include the changes, and develop methodologies of prospection and petrophysical characterization of carbonates. Additionally, our goal was to show the integration of core and log scale data.

Laboratory experiments mainly comprised the results of the routine core analysis RCA, or conventional core analysis CCAL, together with mercury injection capillary pressure MICP, nuclear magnetic resonance NMR, and thin section analyses in the core plug scale. The laboratory data were also supplemented (if available) with the scan data from the computerized tomography CT in the micro-scale.

Wireline logs were divided into two main groups: standard, older ones, such as triple combo logging set, and newer ones such as resistivity and acoustic imaging, NMR log, dipole shear sonic imaging DSI log, geochemical logging tool GLT, or sometimes used more sophisticated dielectric log, or multi-array resistivity device.

3.1. Laboratory Experiments on Reservoir Quality

Ehrenberg et al.'s [46] results, widely discussed in the previous section, could also open the current section. Data used by the Ehrenberg team [47–55], i.e., porosity, permeability, and grain density, were obtained in various laboratories, but using the standard industry techniques on 1 inch plugs, taken from boreholes cores, and outcrops [46]. For the majority of samples, porosity was obtained by helium injection, or weight and volume measurements, and permeability by pressure differential during nitrogen flow. Similarly, mineral abundances were estimated from a combination of petrographic observations on the thin sections, and bulk chemical analyses. For the selected samples from the Finnmark platform (Figure 5), the proportion between calcite, dolomite and noncarbonated minerals was established by X-ray diffraction analysis, XRD. Next, the information was interpolated using grain density, and macroscopic core description. For the Madison samples, the mineral proportion was estimated from grain-density values, assuming presence of only calcite and dolomite. For the Asmari plugs, share of calcite, dolomite, quartz, clay, and anhydrite was obtained from thin section qualitative observations. Then, bulk chemical analyses were performed on the selected samples for confirmation of the results. For all samples, the result of testing the reaction with HCl was the primary information. The example presented by Eberhard team [46] showed how important it is to establish the proportion of lithology components and their influence on reservoir parameters.

Discussing the fracture estimation on the base of thin section examinations, and outdoor observations in outcrops, we first showed the oldest, traditional methods [57,58]. Porosity determination in a system consisting of matrix porosity and fractures may be decisive in reserves determination and the final production of hydrocarbons. In a fracture system, the pore space can be considered as a function of block size, frequency of fractures, and fracture width. A geometrical scheme of a fracture porosity calculation is shown in Figure 6a. "The arbitrary assignment fracture width of 254 μm resulted in the porosity of 1%; the permeability of this fracture was about 54 D [57]". Reiss proposed one simple method for calculating fracture porosity [58] (in [57]). Geometrical models are presented in Figure 6b to illustrate an arithmetical approach to fracture porosity Φ_f calculation. In this method, attention was focused on the relationship between volumes of matrix and fractures. In Figure 7, an explanation is shown of why mathematical calculation according to the scheme presented in Figure 6 was strongly dependent on the size of sample. Low fracture porosity is observed when fractures with large widths occurred in large block sizes. Additionally, extensively fractured rock (with very small fracture widths) in small blocks revealed low porosity values. The graph in Figure 7 shows the porosity decrease with block size increase.

A more precise method of calculating fractures on thin or polished sections presented Stadtműller [59]. Fracture porosity and fracture permeability were split into two fracture groups according to width. In the micro-group, the porosity (PORmfr [%]) and permeability (PERMmfr [mD]) were determined by the inspection of thin sections for fracture widths < 0.1 mm. In the meso (mezzo) group, data were collected of the porosity (PORpfr [%]), and permeability (PERMpfr [mD]) with aperture > 0.1 mm, determined from the analysis of polished sections. Total fracture porosity (PORfr [%]), and total fracture permeability (PERMfr [mD]) were calculated as the sum of data from the micro, and meso (mezzo) groups. Moreover, the helium pycnometry and mercury porosimetry measurements were realized in laboratory to estimate the total porosity (PHIt [%]) and effective porosity (PHIef [%]) for each sample. The methodology of estimating the above parameters, named the "random traverse method" by the author, was described by Paduszyński [60] (in [59]). In this method, a microscope (in case of the thin sections), or a projector upgraded with a millimeter grade (in case of the polished sections), was successfully utilized to estimate the density and width of the fractures. Here, authors also emphasized the thin sections photomicrographs (thanks to side wall cored plugs), which were utilized for microfacies analysis, and fractures identification by Gamal et al. [61]. This important paper, acting as a kind of a link between older and novel methods, is discussed below.

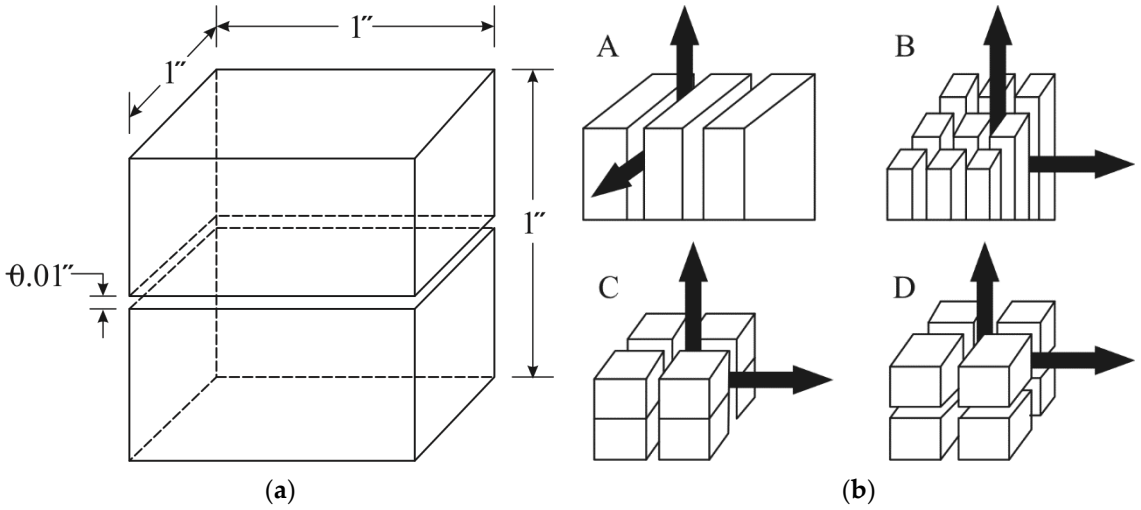

Figure 6. (**a**) Geometrical scheme of a fracture porosity calculation; porosity = 1%, permeability = 54 D (modified after [57]). (**b**) Typical fracture network used for simple calculation of fracture porosity Φf; for A: Φf = b/a, for B and C: Φf = 2b/a, for D Φf = 3b/a, where: a-matrix size (cm), b-fracture width (mm) (modified after [57]).

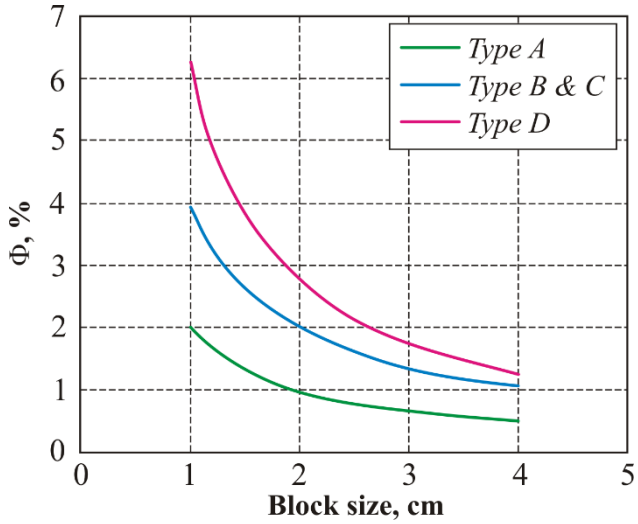

Figure 7. Fracture porosity vs. block size for fracture models presented in Figure 6. (Modified after [57]).

3.2. Conventional Well Logging Evaluation of Petrophysical Parameters

Conventional logs were used from the very beginning, and are still the base technology useful for detecting and describing naturally fractured reservoirs. No single log can accurately describe the fracture network and geometric parameters, and because fractures influence the readings of all logs in different ways, it is convenient to use several logs and combine the results. Indirect but continuous along the geological profile well logging methods are perceived as relatively cheaper and quick in measuring and processing, but not very detailed, and burdened with borehole environment errors. Simple characteristics of log readings are useful in selecting the borehole measurements to identify fractures: their position on the borehole wall, diameter and height, type and filling, i.e., closed, mineralized, open, and also type of fluid in the open fractures (hydrocarbon, water). Integrated interpretation of available readings from the logs, such as gamma ray or spectral gamma ray, resistivity, neutron porosity, bulk density, photoelectric factor, dipole shear sonic imager, caliper, resistivity or acoustic imaging, enables natural fracture identification. In the open fractured zones, the bulk density curves usually revealed small anomalies

due to the drilling mud, formation water or hydrocarbons, which are low-density media. The neutron porosity increases when fractures are filled with liquids, and decreases in the presence of gas, while the sonic transit interval time increases in the presence of fluids. These anomalies occur only if the open fractures apertures are high enough to allow their detection.

Sometimes, atypical drilling data can be added to well logging results. For instance, barite in the drilling mud creates additional bulk density anomalies. During circulation, barite is taken along the wellbore path, and penetrates the open natural fractures increasing the bulk density of fracture. Barite can also become a part of a mud cake, and causes a high readings of photoelectric factor (litho-density log).

Detection and description of fractured reservoirs may be easier when including and combining all available data from wellbore logging, testing, and laboratory measurements.

Several examples of identification and characterization of fractures from the Eocene carbonate formation built of bedded limestone, such as fossiliferous, pyritic, and argillaceous fractures, with chert bands, deposited in shallow shelf marine conditions in the Gulf of Suez, were presented by Gamal et al. [61]. The authors used only conventional logs: caliper, gamma ray, bulk density and density correction, photoelectric factor, neutron porosity, resistivity from the MSFL log, and sonic log. Photomicrographs of the thin sections from the side wall cored plugs were added for microfacies analysis and fracture identification. Fracture aperture observed in the photomicrographs showed values in the range of 10–100 μm; those observed in logs were of a larger order. The authors suggested using conventional logs, and presented a short description of log anomalies. Next, they described in detail examples of individual fractures identified on the basis of well log anomalies, and supported these with thin-section photomicrography. The paper by Gamal et al. [61] is a kind of primer for using conventional logs and thin sections for fracture detection and description.

3.3. Advanced Well Logging Evaluation of Petrophysical Parameters

Important role in natural and induced fractures characterization is played by relatively novel in well logging, various types of borehole imaging logs. Resistivity imaging techniques (for instance, FMI—Fullbore Formation Micro Imager, XRMI—X-tended Range Micro Imager, OBMI—Oil-Base Micro Imager) and acoustic imaging (for instance CAST—Circumferential Acoustic Sidewall/Scanning Tool or UBI—Ultrasonic Borehole Imager), besides other logs, are classified as useful tools in fracture characterization along the borehole wall [62–65]. Borehole imaging tools provide images of wellbore on the base of contrast of physical parameters. Resistivity imaging devices evolved from dipmeters, and generally speaking, the resistivity maps of wellbore in the dipmeter measurements and resistivity imaging are constructed from the microresistivity logging outcomes. The difference in the resistivity maps from an imager and a dipmeter results from larger number of resistivity micrologs, and their more precise orientation in imaging devices [66,67]. Diameter and borehole geometry data from both tools are of similar accuracy. Drilling-induced fractures can be identified from resistivity images as pairs of skinny, conductive or resistive (in oil base muds) zones separated by 180°, arranged subparallel or slightly inclined to the axis of the well, while natural fractures tend to cross-cut the wellbore [67]. In the case of resistivity images obtained in the water-based muds, an open fracture can be easily confused with ones filled with conductive material (e.g., pyrite or clay minerals). On resistivity images acquired in oil-based muds, open fractures can appear as dark/conductive, when the resistivity of the drilling fluid is less than the host rocks ones, or as white/resistive parts, when the drilling fluid is more resistive than the host rocks.

Acoustic imaging tools record the amplitude of the return echo and travel time of high-frequency sonic pulse generated in a borehole, and move along a screw motion line [5,63]. The first borehole image tool was the acoustic borehole scanner, called BHTV [64]. This tool, similarly to other acoustic scanners, creates two images, an amplitude image related to the acoustic impedance of the borehole wall, and a travel time image, mainly related to

the borehole diameter/caliper. Natural and induced fractures are treated as bad reflectors of acoustic waves. Induced fractures are visible in acoustic images as narrow zones of low reflectivity, aligned or inclined to borehole axis, similarly to those from electric images. Open natural fractures in the case of acoustic imaging can be confused with those filled with different materials, because of their detection based on acoustic impedance. Acoustic imagers are used mainly in hydrocarbon prospection, but now, these tools also work in geotechnical exploration, because they turned out to be superior in detecting fractures and thin weak layers. CAST logging sample in Jurassic carbonates is presented in Figure 8 [68]. Fracture traces were interpreted on the base of the CAST record, while their orientation was obtained from the dipmeter.

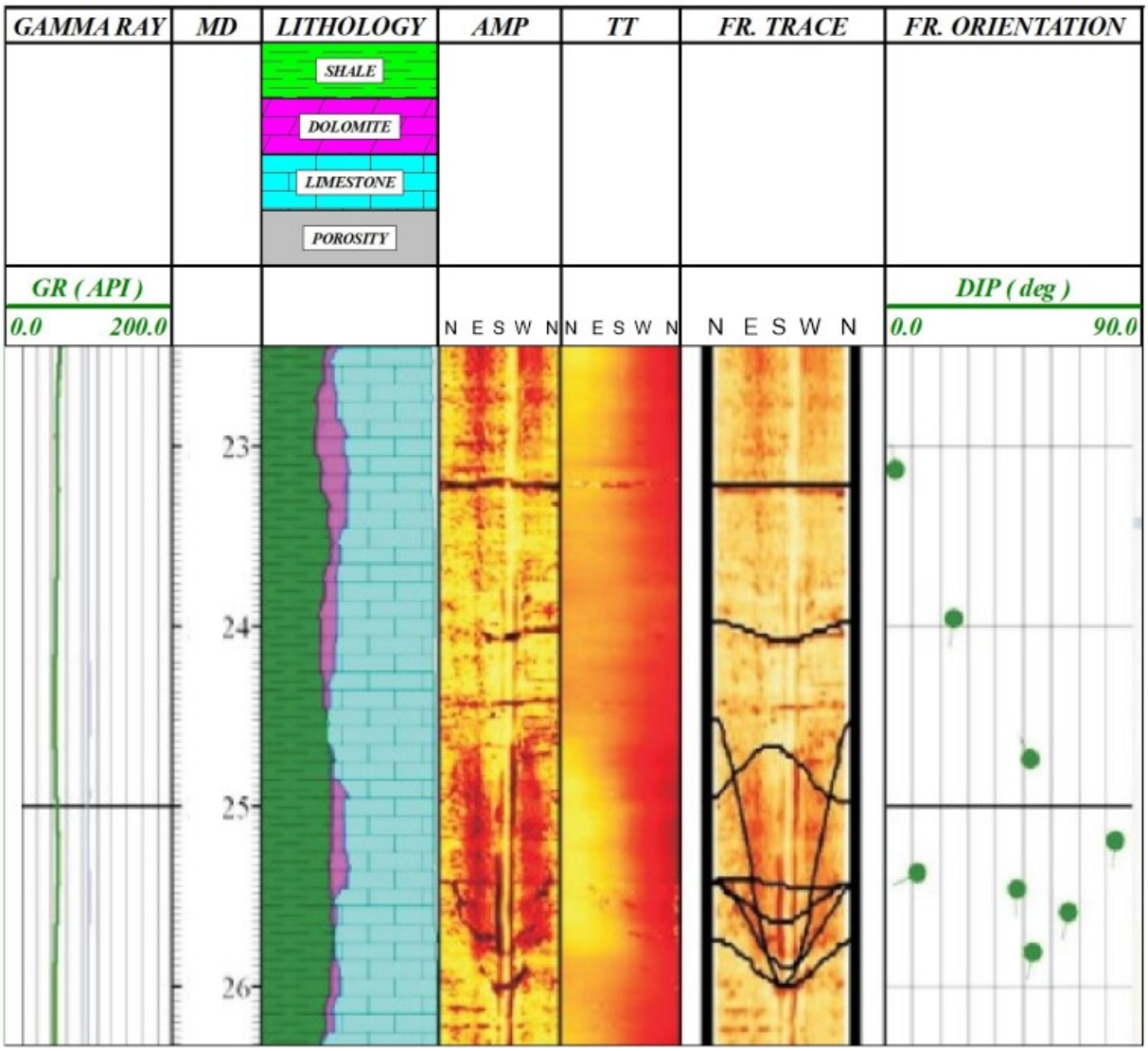

Figure 8. Acoustic image of single fractures recorded by CAST (Halliburton); sample of the Jurassic marly limestones [68]; the first track (from the left)—GR, MD—measured depth; lithology solution (green—volume of shale/marl, violet—dolomite, blue—limestone); AMP—map of amplitude (energy recorded by CAST); TT—map of time—the horizontal scale magnified three times); FR. TRACE—interpreted slides of fractures; FR. ORIENTATION—dips calculated from CAST recordings using Interactive Petrophysics 3.5 software.

The example illustrating the usefulness of dipmeter, SED, and resistivity imaging, XRMI (Halliburton; Houston, USA, Geofizyka Toruń S.A; Toruń, Poland), in characterization of carbonates is presented in Figure 9 [69]. Bedding and fractures were interpreted

from the XRMI images. Dips and azimuths from the SED were presented as the results of processing with different parameters selected by interpreter to make easier geological interpretation of sedimentary events in the geological environment. Various parameters used for SED data processing (correlation interval, step, and angle of correlation [70]) showed that the information could be obtained at different levels of detail. A comparison of results from XRMI and SED showed that the information was complementary. The resistivity map from SED and static or dynamic images from XRMI are comparable. Bedding is distinctly visible in the SED resistivity map.

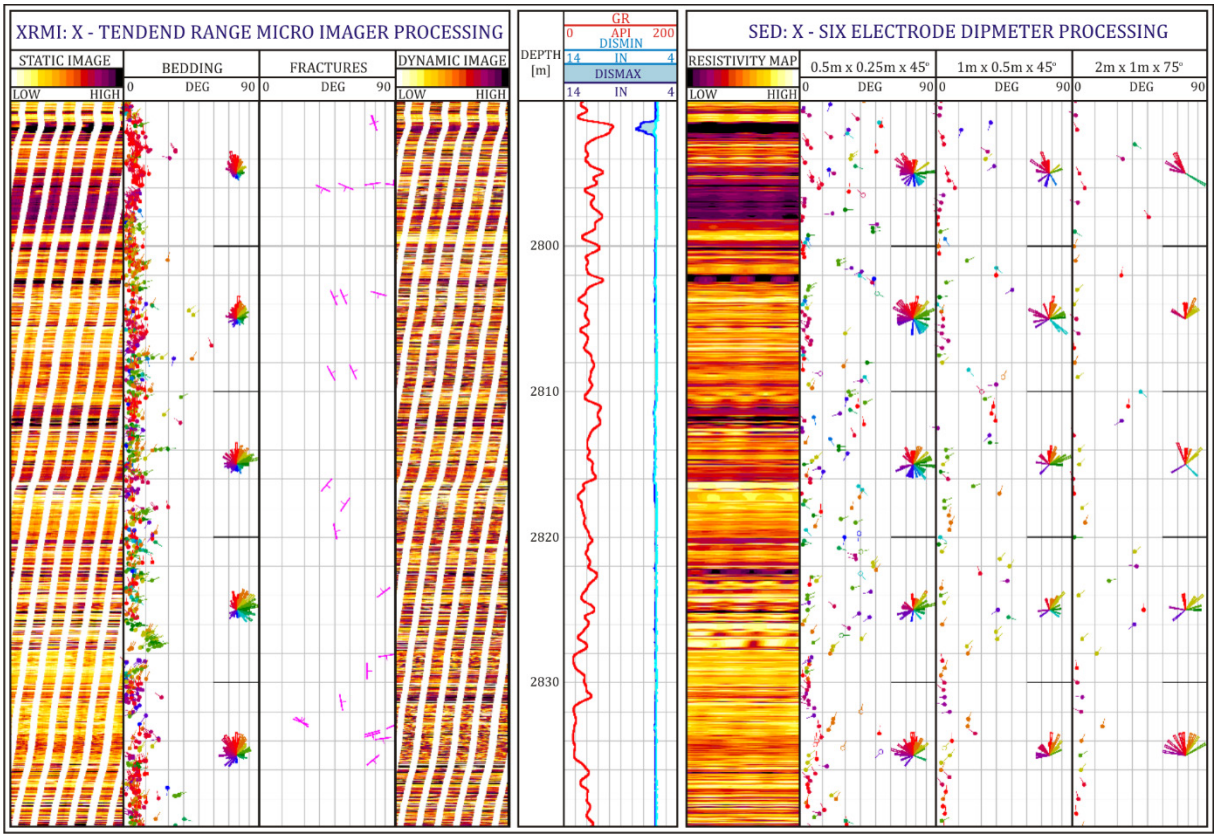

Figure 9. Sample of XRMI (**left**) and SED (**right**) plots after processing; Muschelkalk, carbonates; bedding is distinctly visible in the static image of XRMI (first track) and Resistivity Map from SED (seventh track); dips are presented as colored vectors in the second track—XRMI and eighth-tenth tracks—SED; colored azimuth roses (second track—XRMI and eighth-tenth tracks—SED) show the dominating dips and azimuths; groups of fractures resulted from processing of XRMI image are in the third track; depth is marked in the fourth track; in the fifth track—GR and two calipers—DISMIN and DISMAX are presented; results of SED processing with different parameters are shown in the next tracks: eighth—0.5 m/0.25 m/45, ninth—1 m/0.5 m/45 and tenth—2 m/1 m/75; color scale in the static and dynamic images and resistivity map is related to lower (darker) and higher (lighter) resistivity [69].

In many cases, it is almost impossible to detect open natural fractures using only high-resolution borehole images. The way to comprehensively characterize natural open fractures in a wellbore is a fully integrated interpretation based on all available logs, and drilling data. While standard acoustic log, recording only P-wave slowness, DT, could not sufficiently help to identify fracture, Stoneley wave provided complementary information about type and parameters of fractures [71], despite the limitations related to erroneous interpretation of bed boundaries and washouts as natural open fractures [72,73]. Stoneley wave can be utilized in the qualitative interpretation due to the specific chevron-like interference patterns observed on the recorded full waveforms helping in the fracture

identification [71], and also in determining permeability as a continuous value along the geological profile. Haldorsen et al. [74], in their extensive discussion, described the relations between the Stoneley wave parameters and rock permeability. The method utilizing the Stoneley wave from the high-frequency source needed shear wave velocity and bulk density of formation. The method based on the low-frequency Stoneley wave used wave attenuation between records from near and far receivers [73]. Additionally, agreement was observed between low-frequency Stoneley wave permeability, production log data, and core data [75]. Papers published in the late 1980s and 1990s, in times of intensive development of acoustic logs (including imaging), still offer important positions in the porosity/permeability and dynamic elastic properties determination.

Rajabi et al. [76] enriched standard triple combo logs with a Dipole Sonic Imager and NMR log to get shear wave velocity and nuclear magnetic parameters. Effective porosity (total porosity corrected by shale volume) was determined from NMR spectra. Several interpretation scenarios were presented, starting with the model using only the conventional set of data; next new measurements were added (DSI and NMR). The calculated porosity of each scenario was plotted against core porosity. The determination coefficient R^2 was a measure of the improvement of the interpreted results. Effective porosity from NMR log turned to be a more important factor than shear wave velocity. Both examined parameters caused the calculated porosity to be closer to the core porosity (Table 1).

Table 1. The results of the [76] experiment with adding the modern logs to standard triple-combo for determining porosity of carbonates.

Scenarios	Average Calculate Porosity	Determination Coefficient R^2	Average Core Porosity
Scenario 0—only triple combo logs	7.09	0.78	12.04
Scenario 1—Scenario 0 + DSI	8.61	0.79	
Scenario 2—Scenario 0 + NMR	9.30	0.81	
Scenario 3—combination of Scenario 1 and Scenario 2	9.80	0.83	

Akbar et al. [77] discussed in detail the petrophysical recognition of fractures in carbonates, including two novel techniques, i.e., NMR [78] and Stoneley wave [72] logs, which offered additional ways to calculate the permeability of carbonates. They proved that recorded relaxation time T2 in NMR, combined with the results of mercury porosimetry, increased the chances of indicating the pore size.

T1—transverse, and T2—longitudinal relaxation time distributions from NMR log were the subject of qualitative interpretation at the Upper Jurassic carbonates in the Carpathian Foredeep in Poland to show the depth intervals of increased porosity and permeability [79]. Distributions of relaxation times showed the maxima at different positions on the time horizontal axis. The result of laboratory NMR experiment is presented in Figure 10a with clearly differentiated anomaly positions on the horizontal/time axis. Positions of maxima showed which type of porosity/saturation dominated: bound water (maxima at the lower times), or free water (maxima at the larger times). Different amplitudes of T1, and T2 anomalies (Figure 10b,c) were related to the values of porosity according to the rule: the higher the porosity, the larger the amplitude [75]. Magnified T1 and T2 distributions (Figure 10b,c) distinctly showed the shape and height of the anomalies. The depth fragments of the larger density of maxima in plots (Figure 10d) showed that in those depth sections, an interpreter could expect higher porosity and permeability.

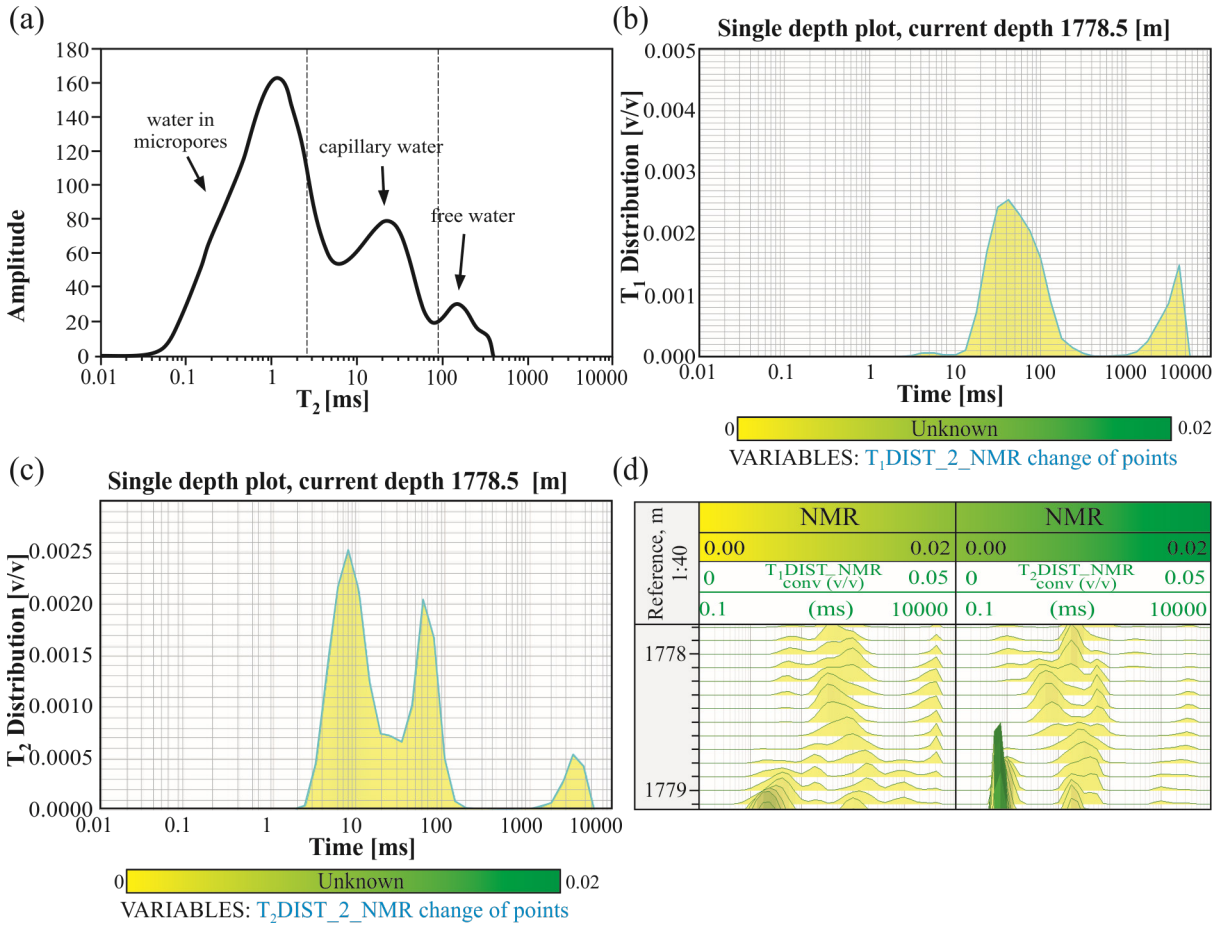

Figure 10. Distributions of T1 and T2 relaxation times (NMR signals) in the Jurassic limestones, (**a**) T_2 distribution, laboratory measurement on the core from the depth section presented at Figure 10d, (**b**) T_1 distribution, NMR log, depth H = 1778.55 m, (**c**) T_2 distribution, NMR log, depth H = 1778.55 m, (**d**) T_1 and T_2 distribution, NMR well logging result at the depth interval 1777.8–1779.1 m [79].

Anhydrite beds in carbonates can be properly determined using the standard logging set, when their thickness is higher than the vertical resolution of the logs. Discrete anhydrite inclusions can be quantified using the geochemical spectroscopy logging tool [80]. Based on the neutron capture and inelastic neutron scatter results, recorded in the spectral logging tool, elemental analysis for the carbonate matrix was processed. Correct designation of the volume of anhydrite allows an increase in the accuracy of porosity, and mineralogy determination in the comprehensive interpretation of well logs. Sulfur and magnesium volumes acquired from the geochemical spectral logging tool outcomes enable proper calculation of dolomite and anhydrite volumes in the matrix, and significantly improve porosity and saturation computation [80]. Al-Shehhi et al. [81] presented a properly designed logging acquisition and advanced interpretation workflow to improve reservoir evaluation in case of carbonates. They utilized elemental spectroscopy (geochemical device) to take to higher-level lithology determination, and used nuclear magnetic resonance and borehole imaging to calculate permeability. Finally, dielectric measurements were used to verify the Archie parameters. Al-Shehhi et al. [81] also proved how core examinations, and borehole tests could be utilized to validate the borehole logging and interpretation procedures.

Ramakrishnan et al. [82] presented the workflow for acquisition and interpretation of well logs as: nuclear magnetic resonance, borehole images, full waveform acoustics, array resistivity, and dielectric. They added neutron capture spectroscopy logs for lithology and porosity evaluation in carbonate reservoirs with anhydrite, or other admixture minerals. The authors showed that the processed methods allowed the improved determination of

lithology, porosity, and pore geometry. Additionally, the results of the determination of petrophysical rock types, fluid saturation, and relative permeabilities were included to obtain the more detailed description of reservoir. They recognized almost homogeneous reservoirs with a few stylolites visible as high-resistivity and high-density thin layers. Permeability was improved on the basis of NMR log.

The determination of stylolites, named as large scale features, important to proper porosity determination, was also presented by [77]. They stated that mapping the carbonate reservoir at a large scale by using well logging measurements at a small scale (borehole imaging) was the real challenge for reservoir geologists and petrophysicists in facies characterization, due to presence of fractures and stylolites. Stylolites, easily recognized in cores and outcrops, were treated as permeability barriers causing an anisotropy in fluid flows. Recognized also as geological factors increasing the porosity, they were intensely sought in well log pictures. Borehole imaging turned out to be very useful in stylolites' recognition and description.

3.4. Computer Modeling, Deep Learning and Artificial Intelligence Application on Petrophysical Parameters

Aperture size or fracture width is one of the basic parameters influencing reservoir permeability. It is important to determine this value to understand the production in fractured formation [2,20]. Ghoochaninejad et al. [83] proposed a novel method of fracture aperture estimation from well logs, utilizing the teaching–learning-based optimization algorithm (TLBO) as the artificial intelligence technique, created for reservoir parameters estimation. At the beginning, authors defined the hydraulic fracture on the base of mechanical fracture, and consequently operated this concept. Ghoochaninejad et al. [83] cited several works, in which authors proposed various ways to determine aperture size, among others, utilizing NMR, multiaxial electromagnetic induction logging, X-ray micro-computed tomography, and also the detection of fracture width by using conventional well logs (Nakashima and Kikuchi, 2007; Wu, 2013; Ramandi et al., 2016 and Shalaby and Islam, 2017 (all in [83]). The method proposed by [83] was an integration of fuzzy inference system and teaching–learning-based optimization algorithm (TLBO). The authors clearly presented the basic structure of fuzzy inference system, and the flowchart of the proposed hybrid TLBO–fuzzy inference system (TLBOFIS). Electrical micro imaging (EMI) log, together with the conventional well logs, provided the data for initializing the fuzzy model. Image log readings were processed using CIFLog—GeoMatrix software, in order to obtain natural fractures, bed boundaries, and faults characteristics. Next, the authors utilized the relationship between mud resistivity and resistivity of invaded/flushed zone, and fracture aperture size in the conductive mud environment [84,85]. Subtractive clustering and Fuzzy C–Means methods of clustering were used to determine the fuzzy rules. The Gaussian membership function showed the best fit to the input well logs: RHOB, NPHI, DT, and LLD (deep resistivity). Various optimization algorithms used the same database for evaluating the methods. Cross-plots between the measured and estimated values of aperture size for each method, with determination coefficient treated as a measure of goodness were the final results. Permeability was estimated on the base of 'cubic law', providing a simple relationship between the hydraulic aperture of a fracture and its permeability [86]. Measured permeability (from core test data), and estimated permeability showed a strong relationship with the determination coefficient equal to 0.82. The proposed method is a challenge for petrophysicists, because it requires knowledge of novel statistical, and machine learning techniques. However, in our opinion, it encourages the creation of interdisciplinary teams, and promises satisfactory results.

Watanabe et al. [87] contributed to computer-modeling the fracture aperture incorporating experimentally determined fracture surface geometries, fracture permeability, and fluid flow from rock fractures under confining pressures. Using the results from the cited literature, and from their own experiments, authors stated that fracture permeability changed with confining pressure, and also with shear displacement. Based on the flow-

through simulation, the model permeability was evaluated. The same equations were used as ones employed for the flow investigations. At the end, the determined permeability was successfully juxtaposed with the measured fracture permeability.

In several papers, the computer X-ray tomography CT was mentioned as a useful tool in the carbonate characterization. In the literature, papers utilizing computer tomography are observed since the early application of CT technology in petrophysical investigations to the current publications [87–93]. Computed X-ray tomography enabled the 2D and 3D analyses of pores and fractures, providing the qualitative, and quantitative characterizations of pore space, and revealing rock filtration abilities. Based on the processed computer images, standard parameters such as pore diameters, microfracture apertures, porosity, and total pore area could be determined [94,95], whereas advanced parameters, defined on the 3D images, for instance, global pore connectivity (global average pore connectivity), reflected the pore space development degree (pores, fractures, pore channels), in which reservoir fluid could flow without disturbances [92]. New filtration parameters were focused on describing rocks' ability to hydraulic fracturing, as well as recognized paths of fluid flow. Novelty in computer tomography technologies oriented on determination of petrophysical details from very small rock samples were developed in parallel with the machine deep learning, and artificial intelligence applied for clustering the well logging data, and solving the reverse problem in fractures characterization.

Extending the idea of artificial intelligence used in petrophysics, one more example was dedicated to the estimation of density of fractures from the standard well logs using an adaptive neuro-fuzzy inference system [96]. The neuro-adaptive learning techniques used fuzzy modeling procedures to learn information about a dataset. The membership functions allowed controlling the input/output data. Subtractive clustering [97], according to the Zadeh [98] concept of partiality, was the effective method for constructing a fuzzy model. Models for discrete and continuous data were presented. Data were prepared in two steps: determining the fracture densities per meter of the borehole wall from the image log (ultrasonic borehole imager (UBI) and oil-based mud imaging tool (OBMI)), and classification of fracture densities to three classes: 0–2 fractures per meter, 3–4 fractures/meter, and more than four fractures per meter. Normalized fracture density was cross-plotted vs. bulk density (RHOB), acoustic slowness (DT), neutron porosity (NPHI), and deep resistivity (Rd). All log data were linearly normalized, because fuzzy models were highly dependent on the clustering process, the spatial shape of the clusters, and their statistical properties. Clustering radii, being the controlling parameters for determining the number of fuzzy if–then rules, were the measure of quality of the models. The models were tested on the data from nine wells of the Asmari formation (Iran), and the average fracture density map for reservoir interval was constructed. It was worth focusing on the methodology, and presented results to explain many details, necessary to understand the application of fuzzy logic in fracture determination. Methods utilizing computer modeling, deep learning, and artificial intelligence in combination with laboratory and well logging data are still developed to improve permeability determination [99]. In our opinion, and in the opinions of the other above cited authors, the novelty in fractured carbonates interpretation is using the machine deep learning techniques, and artificial intelligence to combine the super detailed data from X-ray computer tomography, and similar sophisticated laboratory technologies with continuous well logging measurements.

3.5. Well Logging Outcomes vs. Laboratory Results

In our considerations on fracture porosity, Ekofisk chalk [34] was an example of carbonate formation, in which the typical model of permeability–porosity relationship from core data could not be applied. The algorithm for the permeability estimation in this case was built on data from logs, cores, and well-tests. However, fracture spacing extracted from cores was the main information. The relationship between fracture intensity, i.e., degree of fracturing, and effective permeability was the first step in the algorithm. The next step was establishing the relationship between fracture spacing (from core data) and

chalk petrofacies (from logs). Six petrofacies (homogeneous chalk, pebble floatstone, burrowed homogenous chalk, laminated chalk, burrowed laminated chalk, and burrowed argillaceous chalk) were extracted using the clustering technique, which statistically assigned core-described lithofacies to log characteristics. Porosity, shale volume, and activity, i.e., absolute value of the first derivative of the microresistivity log, worked as indicators of facies. Natural fractures recognized on cores were classified into five types: tectonic, stylolite-associated, slump-fractures, irregular, and healed fractures. All of them enhanced reservoir permeability with exception of healed ones, which could reduce matrix permeability [34]. Fractures enhancing permeability were completely or partially filled by secondary mineralization, frequently by calcite. Petrofacies were grouped into three distinct categories, based on general chalk type: Category 1—argillaceous, laminated chalks, 2—bedded chalks, 3—massive chalks, and a relationship between them and fracture intensity was established. Histograms of fracture intensity in the lithology categories showed that the tectonic fractures were dominant (Figure 11). Next, the authors found a method to translate the fracture intensity values into estimates of effective permeability. They modified techniques developed by Da Silva [100] and Thomas et al. [101], showing that by grouping fracture spacing from core data into presented categories, a correlation between effective permeability and fracture spacing could be determined. This correlation was the base for the processed and implemented algorithm. Building the algorithm authors anticipated difference in flow capacity by assigning more contribution to the tectonic fractures relative to the stylolitic fractures. The relative proportion was determined through calibration of core fracture data, and PLT distributing well-test permeability. Validation of the algorithm was completed in two stages: (i) involving permeability determined from well-test data, and (ii) geostatistical techniques. In the authors' opinion, the presented solution was an important step towards permeability mapping in the carbonate reservoir [34].

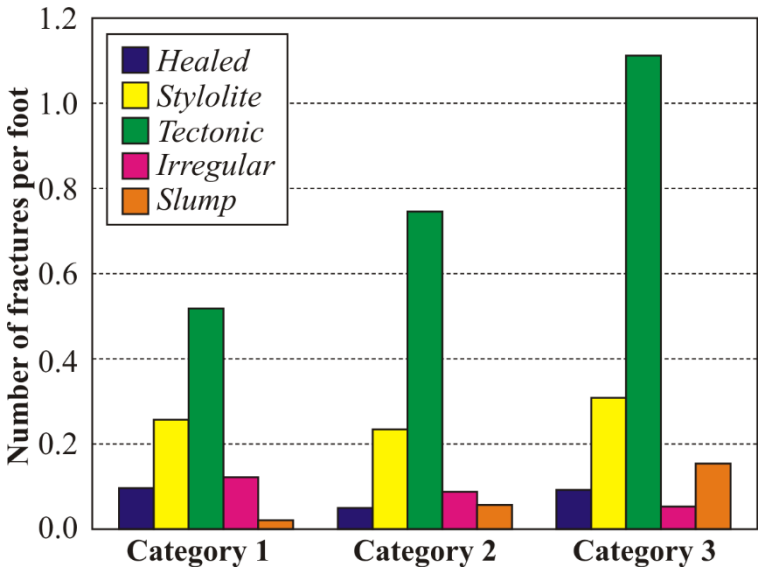

Figure 11. Fracture intensity vs. petrofacies group, Ekofisk formation (modified after [34]).

Another approach was presented by Stadtműller et al. [91] on the basis of laboratory, and well logging data from the Zechstein Main Dolomite formation in the Polish Lowland. The standard interpretation of the petrophysical parameters available in the borehole data set, including PHI log as an effective porosity estimate, as well as K, as an absolute permeability estimate. The laboratory core data were obtained from different depths. Due to this, the PORO values for PHI, and PERM values for K were selected from the results of well logging interpretation at the depth as close as possible to the depth from which samples were taken, separately for micro- and mezzo-fractures. Microfracture-porosity index and mezzofracture-porosity index were the quantities defined for scaling the fracture perme-

ability of the analyzed rocks compared with the porosity interpreted from well logging. The relationships between permeability and permeability index for three defined classes (micro-, mezzo- and macro-pores) revealed high determination coefficients (Figure 12). Points scattering in Figure 12 illustrated the difficulties in depth matching between thin sections, and well logging interpretation results. Based on the fundamental paper of Luthi and Suihaite [84], considering the fracture analysis, and aperture calculation, the automatic procedure in the domestic system for the processing, and interpretation of well logs Pro-Geo [102] was processed and implemented. The procedure consists of the following steps: (i) canceling of the breaks between pad registration to obtain homogeneous vector data, and vector curves COMPACT, (ii) fracture tracing using the filtration and skeletonization procedures to obtain vector curves FRACTURE, and FR_SKELETON, (iii) calculating the aperture of recognized fractures to obtain vector curves FR_APERTURE. The results of the abovementioned procedure in the ProGeo system including Fracture Porosity Index (FPI) are presented in Figure 13. In the selected depth section single porosity data from the laboratory measurements were available. Good agreement between laboratory data PORO_lab and matrix porosity MATRIX_P proved the correctness of the interpretation.

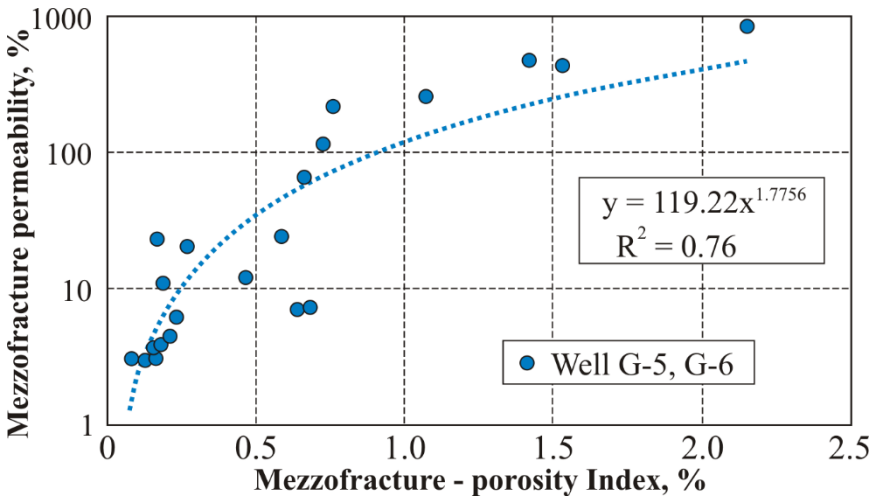

Figure 12. Relationship between mezzofracture permeability and mezzofracture-porosity index [91].

The FPI is defined as the ratio of the surface occupied by the traced fractures to the total surface of the analyzed borehole wall. The FPI values in the presented sample are in the range of 0–0.03 [91]. Relevant correlations between rock porosity, and fracture porosity and permeability were calculated on the base of the results of laboratory and well logging measurements and interpretation. The described calculation sequence led to final result, i.e., total permeability being the sum of micro-, and mezzo-fracture permeability and matrix permeability enlarged with macro-fracture permeability [91]. The results of the described analytical procedure, especially the obtained aperture distribution of the analyzed fractures, can be used as the input data for the construction of the models of fracture formation using algorithm DFN (Discreet Fracture Networks) [68]. The presented example illustrated the approach of the authors of the review paper to combining data from cores and logs, and scaling the results.

The Archie equation is widely used in the water/hydrocarbon saturation in the manual approach, and computational industry systems of well logging interpretation, but there are many constrains, which lead to erroneous estimates of water saturation. Ramamoorthy et al. [103] proposed a modified methodology, based on the Archie approach, introducing the effective resistivity model of an inter- and intra-granular vuggy carbonate. The positive result, i.e., proper hydrocarbon saturation, was obtained on the base of open hole logs and/or core data. For multipore systems, Petricola et al. [104] included a sequential method utilizing the Archie equation for a rock divided into three parts. Ramamoorthy's team [103]

proposed a solution for a rock partitioning according to porosity similar to that of [104], and introduced the "effective conductivity" based on the homogenization methodology proposed by Ramakrishnan et al. [105,106]. The model comprised microporous grains with intra-granular porosity Φμ, intergranular macro-porosity, Φm between the grains, and vugs, Φv, being the results of grains dissolution (Figure 14) [104]. Three components of porosity may be obtained using optical, and scanning electron microscope (SEM), petrography description, or from NMR, and/or electrical images as proposed Ramakrishnan et al. [105]. Mercury injection pore-size distributions, supported by petrographical recognition, could be recommended as relatively inexpensive sources of information on the pore partitions.

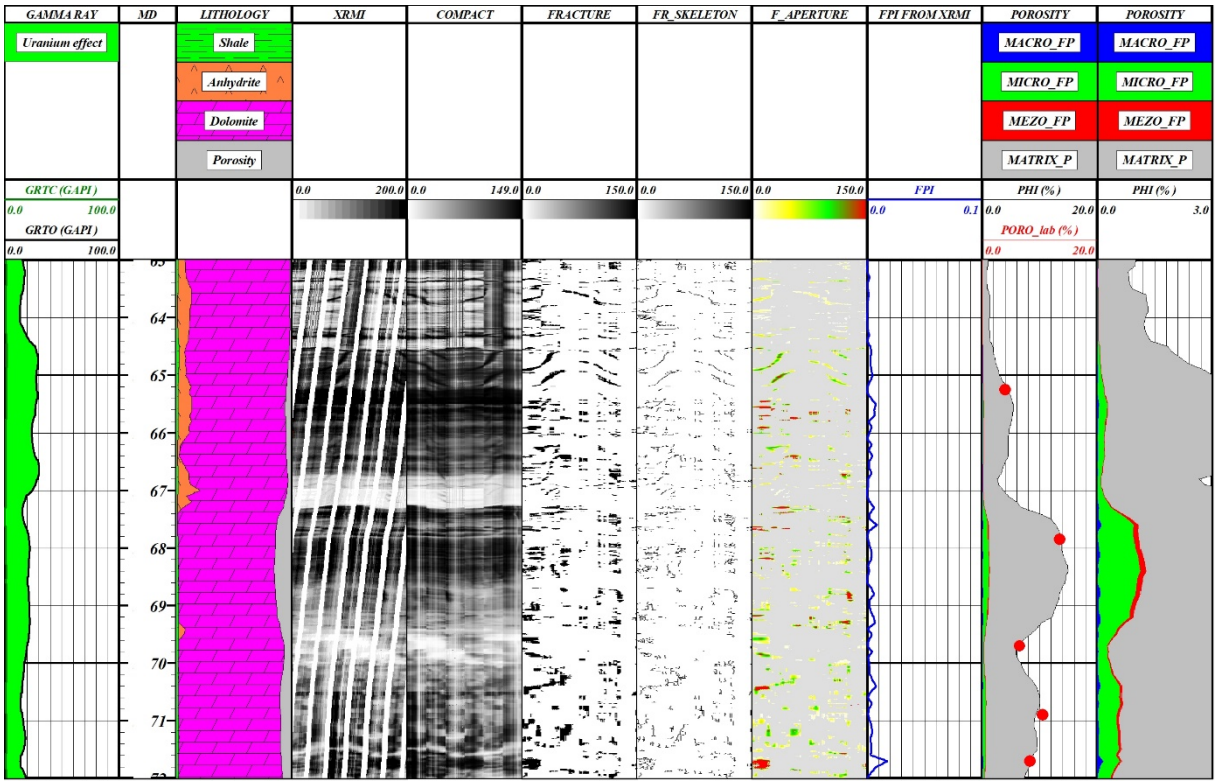

Figure 13. Results of the processing and interpretation of electric imager log for macrofracture determination in the selected depth section of the main dolomite, Poland: GRTC—gamma ray log without uranium component, GRTO—total gamma ray, MD—measured depth, changed, FR_—fractures; FPI—fracture porosity index, MACRO_FP, MICRO_FP, and MEZO_FP—macro, micro and mezzo fracture porosity, respectively, and MATRIX_P—matrix porosity, red points—PORO_lab in the last two tracks—laboratory porosity [91].

Ramamoorthy et al. [103] proposed the formulas for all types of porosity using the m cementation factor, like in the Archie formula. In theory, this factor is different for the intra-, and inter-granular pore systems. However, in practice, a single value was used. Additionally, the same saturation exponent n was used for both intra-granular and intergranular pore systems. Each pore system was only filled to its residual water saturation. Hence, the authors considered the resistivity of vugs filled with hydrocarbon and brine (the rest of vug), the resistivity of intergranular porosity filled with hydrocarbons to residual water saturation level, and intra-granular porosity, also filled with hydrocarbon and brine up to residual water saturation level. Total water saturation was the sum of each component. Such reasoning was provided for resistivity logs of short, and deep radius of investigation operating in the flushed, and uninvaded zones, respectively. On the basis of elaborated formulas, analytical modeling of n and m was conducted, and final values were verified comparing the results of laboratory measurements of these parameters on the cores from the well. As a result, the authors constructed the effective medium model

for water saturated rock, and HC saturated rock, and tested it in aspects of: petrophysical consistence, primary drainage, water intrusion, and wettability changes. Resistivity index was modeled on the base of assumed formulas, describing relations between resistivity of rock in the invaded/flushed, and virgin zones, porosity, and resistivity of fluid in different part of rock (intra-granular, intergranular, and vugs), cementation, m, and saturation, n factors. The resistivity index was calculated for various volumes of Vμ, Vv, and Vm, and in each case, the following stages were considered: drainage, water flood for water wet, mixed wet, and oil wet formation. Three examples of application of the processed models to well logging data were presented for carbonates drilled in the Middle East, confirming the consistency of the methodology. The following guidance for model input data was presented: (i) partitioning of porosity into Vμ, Vv, and Vm, (ii) assuming the cementation Archie exponent, m, (iii) adoption of residual water saturation, and maximum residual oil saturation, (iv) stipulation, whether the formation could alter wettability to oil-wet.

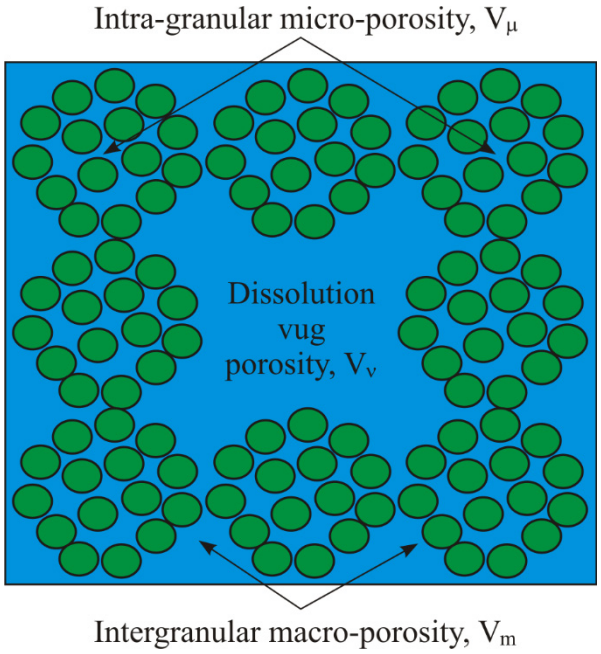

Figure 14. Illustration of pore arrangement (after [103], modified); symbols Vμ, Vv and Vm mean volume of selected type of porosity: intra-granular micro-porosity, dissolution vuggy porosity, intergranular macro-porosity, respectively.

In the review paper, we allocated considerable space for [103], because the described novel methodology, based on resistivity, cementation, and saturation factors, including type of wettability, and residual water and oil saturation is similar to the traditional Archie approach. In the detailed presentation, we wanted to show the continuity of the research on the reservoir properties determination over the decades: Archie, 1952 [45], and Ramamoorthy et al., 2020 [103].

Skalinski and Kenter [107] presented a comprehensive work, showing the links between petrophysical properties, geological attributes, and reservoir features as porosity and permeability of carbonate reservoirs on the base of rock types determined on different factors. The presented workflow is a novel approach because "integrates geological processes, petrophysics and Earth modeling aspects of rock typing, integrates core and log scales, and provides a flexible 'road map' from core to 3D model for variable data scenarios that can be updated with progressive changes in data quality and quantity during the life cycle of an asset" [107]. The authors assumed that "the goal of carbonate rock typing is to properly and realistically distribute log-derived reservoir properties in 3D models, and to generate a spatial distribution of appropriate rock types that control oil-in-place and fluid flow" [107]. They focused their attention at the common understanding/definitions

of discussed parameters influencing the rock types by different specialists, i.e., geologists, petrophysicists, and reservoir engineers, etc., at the interface of geology and petrophysics. The second aspect, important from the petrophysics point of view, was the scale—core scale (in laboratory experiments on cylinder core plugs, and micro-scale in CT investigations), and log scale (with all factors burdening the well logging measurements in borehole). The authors assumed that rock types are scale-dependent. Using their own experience, and citing several dozen literature issues, the authors selected the rock types RT based on: (i) mostly geological (depositional) facies, (ii) pore typing, (iii) integration of depositional facies, diagenetic modification, and pore types, (iv) petrophysical partitioning of core or log data, (v) static or dynamic RT. Detailed presentation of eight steps of the proposed workflow enabled discussing in details an integrating core and log results in different scales by using defined rock types on the cores, and predicting the same RT from the logs. The first step comprised the data scenario, the next five steps—determination of the defined RT, seventh—dynamic validation and eighth—petrophysical rock type model static.

A scheme presenting the steps required for the determination and definition of the petrophysical rock types PRT consists of several loops (Figure 15). The pore typing step is based on varied data scenarios, and integrates pore types from measurements in core and log scales. The authors stated that the most useful data for the appropriate pore type identification was from the mercury injection capillary pressure MICP, providing also detailed information on pore throats sizes used to check flow in the reservoir. The authors also suggested that several types of logs may be utilized interchangeably (if available). The presented scheme from [107] is shown as one of the useful flexible methods, which can be utilized by petrophysicists in their work. Two examples from the carbonate reservoirs (Tengiz Field, Kazakhstan and Wafra Field in the Partitioned Zone (Kuwait—Saudi Arabia)), described in detail in [107], contain practical knowledge on combining the laboratory and log data on the background of rock typing.

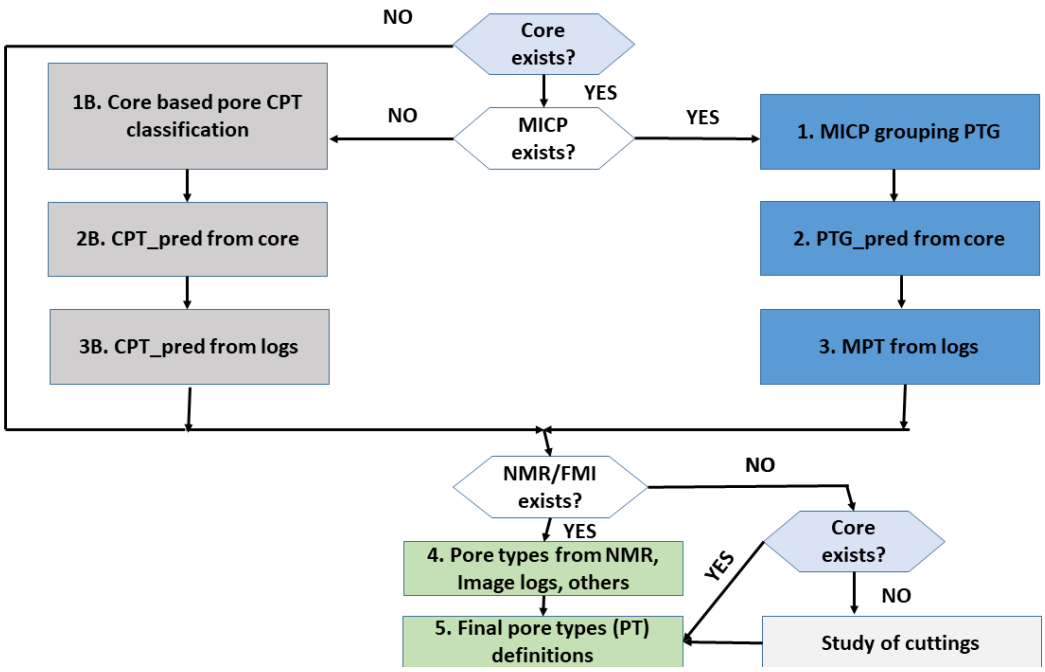

Figure 15. Scheme presenting the steps required for the determination of the petrophysical rock types PRT; CPT—core-based pore types; MPT—multi-logs pore type; MICP—mercury injection capillary pressure; PTG—pore type grouping; PT—pore type; NMR, FMI, image logs—logs which results can be utilized (after [107] modified).

One more example relates to the data from the Barents Sea, close to northern Norway, where the main reservoirs of the Alta discovery consist of a mix of the Paleozoic carbonates

of the Ørn and Falk Formations, and basal Triassic conglomerates [108]. In the Alta area, the lower part of the Ørn Formation consists predominantly of fully dolomitized, cyclic shelf deposits. Reefs in the Alta area were drilled in the early stage of prospection. They were interpreted as a part of buildup complexes characteristic for the latest Carboniferous to Early Permian carbonate deposition in the Barents Sea (Elvebakk et al., 2002 in [108]). Coring and wireline logs (gamma ray, density, neutron porosity, spectroscopy, dielectric, resistivity, sonic, images (ultrasonic and resistivity), nuclear magnetic resonance NMR, and formation pressure FMP) were realized in wells, and sidetracks. Limited number of logs was available in the horizontal production test well. Core measurements on plugs included porosity, permeability, grain density, cementation exponent (m), XRD, MICP, and NMR. Additionally, whole-core measurements were performed on seal peels for porosity, permeability, grain density, and cementation exponent determination. The carbonates of the Ørn Formation were fractured to varying degrees, and with variable porosity–permeability relations. Vuggy dolomites of the Falk Formation represented the main reservoir facies, and were characterized by low porosity, but moderate to good permeability. Although grain density, and cementation exponent were relatively stable, a probabilistic approach to the logs interpretation was applied, and multimineral solver from the IP (Interactive Petrophysics) software was used. To validate the interpretation model, an estimates of grain density, total porosity, and volumes of different minerals were compared to the results of core measurements. In carbonates, porosity from the routine core analysis RCA on 1-inch plugs represented matrix porosity, and micro-fractures. When shaliness was not big, or no shale was observed, one could assume, that the helium porosity from RCA was close to the total porosity. Total porosity from logs with a larger resolution comprised matrix porosity, vugs, and fractures. In the discussed case, the difference between above defined porosities was observed in some sections, so it was decided to measure porosity and permeability on whole-core samples assuming, that those measurements had a vertical resolution closer to the log interpretation. Additionally, a combined MICP-NMR study comparing plugs to logs was performed. Comparison of the NMR results from log to MICP outcomes from plugs in the reef showed, that small pores were revealed by both methods, and showed similar pore-throat distribution. Mega-pores, however, were captured in the logs, but were more or less absent in the plugs. The original figure with original caption from [108] was included in Figure 16 to confirm agreement between the results of NMR log, and MICP experiment in laboratory.

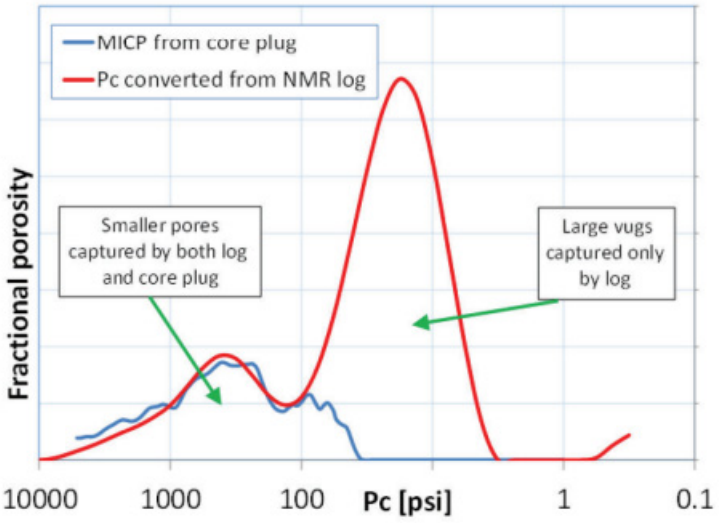

Figure 16. "For display purposes, MICP pore-throat distribution expressed by capillary pressure (Pc) from plug vs. NMR T2 converted to Pc in the Ørn reef. This example illustrates how the plug (MICP) is not capturing large-scale growth framework porosity seen by the NMR log [108]".

The authors in [108] state that in the Alta area permeability from matrix and fractures contributed to production. In some sections, matrix permeability was low, and in such intervals fracture permeability was important. In the reef, matrix permeability was high, and its contribution was dominant. Summing up, authors stated that the results of the RCA on 1-inch plugs represented only the matrix porosity/permeability, and possibly micro-fractures.

We included this paper into the review as representative one, and relatively new for combining core and log data to scale the results.

3.6. Multi-Scale and Multidisciplinary Approach

Two last examples from the previous subsection could be also included to the below presented one. Skalinski and Kenter [107] pointed out several times the necessity and efficiency of combined results from laboratory (core-scale) and well logging (log-scale) data. Examples presented in [107] are good confirmation of the authors' position. Gianotten et al. [108] added the results of whole-core (dozen centimeters) measurements of the petrophysical parameters beside the results of routine core analysis RCA, or conventional core analysis CCAL, and various well log outcomes extending in that way the pool of available results.

Results of permeability study of gas-bearing dolomites on the Lubiatów hydrocarbon deposit (Poland), obtained by the Krogulec team [109] were compared with the results of dolomites permeability determinated in other hydrocarbon deposits around the world. The authors presented the relationships between permeability and porosity, and also between permeability and mineral composition. The results of laboratory tests and geophysical measurements were compared. Additionally, historical laboratory data were processed in order to quantify the permeability variability depending on the depth, and measurement method. Base on the processed data, and using the available, historical results, authors showed, that there was no correlation between permeability, porosity, depth, and mineral composition of dolomites. They revealed, that porosity obtained depended on the method used. The fact, that various methods used for permeability determination provided different results, confirmed the heterogeneity of the dolomite, and showed once more, that methodology of the examination should be appropriate to the purpose of research. The authors also emphasized, that the comparison with the results obtained in different regions all over the world could be highly risky due to many factors influencing reservoir properties. The presented results confirmed the importance and need of detailed diagnosis of the analyzed reservoir in various aspects.

Problem of lithology characteristics and facies recognition was also discussed during the estimation of porosity vs. permeability relationships in the carbonate heterogeneous aquifers [110]. The results of laboratory measurements on numerous collections of core samples showed that the hydraulic properties of the rock matrix were strongly dependent on lithology, and facies. Data subdivision into groups, corresponding to ranges of porosity and permeability, subjected to stratigraphy, lithology, and facies made the determination of the right relationships much easier. Additionally, Bohnsack et al. [110], in the interpretation of petrophysical data emphasized the influence of the diverse observation scales, and detailed information about the rock. The results of investigation of rock properties on a pore scale (microscale—for instance micro-tomography) differed from the properties measured on the core scale (macro-/mezzo-scale—for instance porosimetry) due to the heterogeneity of the rock matrix, particle size, and pore size in different scales. In a regional/basin scale, fractures, faults, results of diagenesis, and lithostratigraphy also influenced the hydraulic abilities of the reservoir.

The issue of heterogeneity and anisotropy in carbonate reservoirs was raised by Rashid et al. [111]. Authors examined the factors affecting porosity, permeability, and reservoir quality in prospective low permeability carbonate reservoir in northern Iraq. Data included regional stratigraphy, outcrop sections, well logs, and core material from wells, and also a large collection of lab results obtained on core plug samples. Based

on available data, formation in the study was divided into three lithological units, two microfacies and three petrofacies. Petrofacies were determined on the base of wireline log data, including porosity from NMR measurements. In the study, 173 core plug samples, from 99 m of core, from several wells were used, together with 95 m of whole outcrop [111]. Routine core analysis was carried out. Additionally, pulse-decay method was utilized for permeability determination on the selected plug samples, because the conventional steady-state method was not effective. Data from macroscopic core observation, and specimens from outcrops, together with scanning electron microscopy results, XRD oucomes, porosity and permeability measurements enabled obtaining the lithofacies, porosity, permeability, and reservoir potential. Well logging data allowed understanding the structure, origin, and evolution of deposit. NMR log was used in discrimination between petrofacies B and C (Figure 17). Easy permeability vs. porosity plot allowed distinguishing between the petrofacies A and others. Peaks observed on the NMR T2 relaxation time spectra in the depth sections helped in differentiation of A, B, and C petrofacies.

In certain portion of the samples, the stylolitisation and fracturing were highly developed and observable, and in others, they were completely invisible. Fractures, including micro-fractures, open fractures, closed fractures, and partially cemented fractures were identified. They could influence fluid flow. Some of them could enhance the media movement in pore space, while others could act as a barrier to the reservoir fluids. Inclined, near vertical fractures, which cross-cut stylolites were observed both in the outcrops, and in the core samples. They were considered as the reason for anisotropy.

Heterogeneous, porous, fractured and stylolite-rich carbonate rocks were thoroughly analyzed by Maniscalco et al. [112]. The authors presented the multi-scale, and multidisciplinary approach due to intrinsic heterogeneity of carbonates, additionally changed with time by diagenesis, and structural discontinuities, which made those rocks very difficult in petrophysical characterization. Faults, fractures, veins, and stylolites, considered as discontinuities in the carbonate reservoirs, were a great challenge in macro scale (macroscopic description of cores, and literature study), but attention was also focused on micro-scale characterization by mesoscopic, and microscopic description of cores and 3D image investigations. Sedimentological, and structural surveys were carried out on 165 m of cores, next 22 thin sections were prepared at different depths from representative cores. Dips and azimuths measurements on cores enabled real orientation of discontinuities (fractures, joints, and stylolites). Frequency of different dip angles, and the number of fractures per linear meter were illustrated on histograms. The results from direct observations of cores, and thin sections were compared to the data from well logs: spontaneous potential, gamma ray, density, porosity, and sonic. Well logs allowed to discriminate four clusters in the analyzed profile, in which juxtaposition of characteristic values of parameters and number of fractures per meter were presented. High GR values helped in discrimination of black shale with organic matter, source rocks important in conventional HC deposits. Results showed, that depositional, and diagenetic processes caused a low residual porosity. Fractures were mainly mineralized thus, they did not contribute to the overall porosity. Stylolites revealed a certain porosity.

Finally, we touched on a completely different application of well logging data. Reservoir engineers and petrophysicists in long horizontal wells use the web based real-time displays for monitoring drilling [113]. It enables obtaining and controlling the collective, collaborative knowledge on the whole wellsite. This real-time data visualization of drilling and geosteering displays any detailed interpretation for Logging/Measurement While Drilling (L/MWD) with high quality images, and special tools like wireline logs, NMR, mud logging, coil tubing, etc. [113]. Based on such data an operator can make timely and more informed decisions regarding the drilled reservoir and compare the current results with ones in the reference well, in the same deposit. In geosteering the results of laboratory methods utilized for lithology determination (for instance X-Ray Fluorescence, XRF) can be also used [114]. Building lithology profile on the base of mud logging in horizontal well,

and XRF measurements carried on the long cores from the reference well, compared with lithology solution in vertical well can be a real, functional support for the drilling operator.

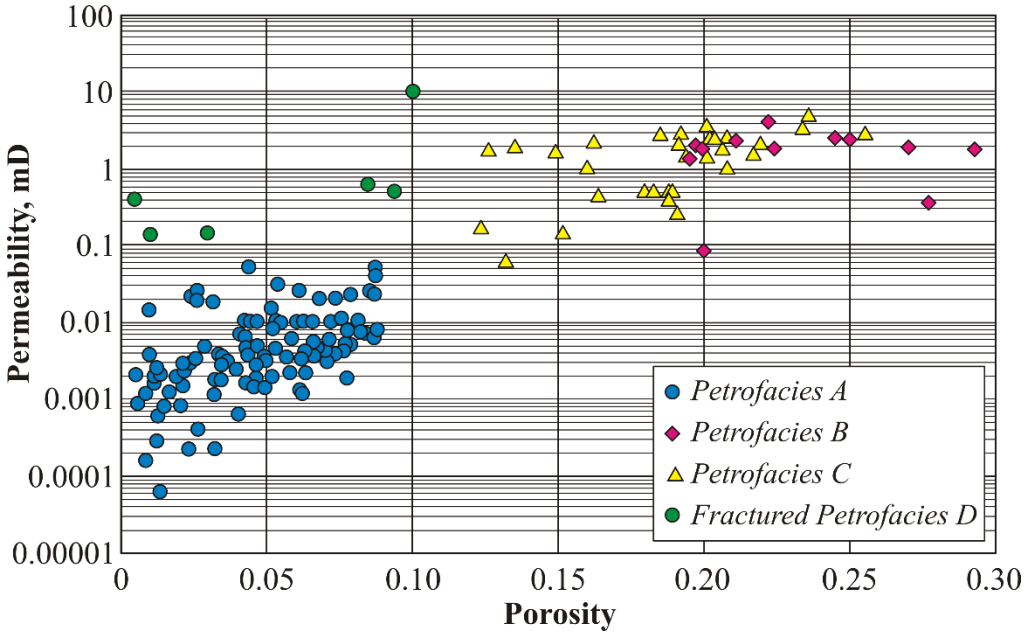

Figure 17. Permeability vs. porosity plot including petrofacies discrimination (modified after [111]).

4. Summary and Conclusions

Presented review was based on the papers arbitrary selected by authors to show the problems encountered by petrophysicists, petroleum geologists, hydrogeologists, and geothermal engineers trying properly interpret well logging data combined with laboratory experiments results to characterize carbonate reservoirs. The goal was to present the achievements of different groups of specialists vs. challenges generated by complicated geological conditions, in which carbonates were deposited, including their burial and tectonic history, and contemporary conditions. The purpose was also to show the novelty in methodology of prospecting for carbonate reservoirs using modern technologies in well logging as NMR, DSI, spectral neutron-gamma geochemical log, and illustrate the advantages and benefits they provided. Direct laboratory results were always used for calibration, and validation of indirect well logging measurements. Results obtained on thin sections (historic) and using electronic microscope techniques (modern) were also treated as independent research. We presented the geometrical approach to visualization of fractures to make the reader aware how difficult fracture analysis was due to heterogeneity of the fractured formations. The examples presented were intended to show samples from different regions, and processed by specialists from countries advanced in laboratory and well logging technologies, and also those who used the traditional methods.

As the first step of the carbonate reservoir parameters characterization, we recommend:

(i) Analyze mineralogical and petrographic features of carbonates, because geology strongly influence the petrophysical attributes of these rocks,
(ii) Be aware of variety of carbonates all over the world, and try to place the considered formation on the background of others, processed by other researchers and engineers to use their experience,
(iii) Examine in details the individual conditions in the processed carbonate, and compare the similarities and differences to the known (literature) samples, when utilizing solutions selected by other interpreters,
(iv) Having in your disposal only conventional logs: caliper, gamma ray, resistivity, bulk density, neutron, and sonic try to use the experience of other specialists, who solved the problem using only limited amount of old data,

(v) Encourage the decision maker petrophysicist to order new well logging measurements to improve the interpretation (for instance geochemical device) and new laboratory technologies (for instance microtomography) to get new information despite of high costs,
(vi) Apply deep data mining to archive well log data using advanced computer technologies,
(vii) Utilize modern software (for instance artificial intelligence, machine learning) to combine laboratory outcomes (micro scale) and field measurements (macro scale),
(viii) Search for advanced (automatic) computer procedures combining apertures from both types of images—microscopic thin sections, and full cores analyses, and outcrops examining, or borehole imaging logs having still in the mind the problem of scale, crucial in these two approaches.

As the second step we recommend:

(i) Use all available well logs and laboratory experiments results to make all mutual correlations to pre-recognize possible relationships,
(ii) Compare the laboratory XRD mineral solution with the outcomes of geochemical well logging to precisely determine the mineral composition of carbonate, especially when anhydrite is observed,
(iii) Order the NMR measurement in borehole and laboratory to improve porosity, permeability and saturation determination,
(iv) Compare the laboratory results of the longitudinal, Vp and shear vs. velocities (and other dynamic elastic parameters) with the results of dipole sonic imager log to recognize influence of depth, and pressure on porous space image,
(v) Combine the results of imaging logs (resistivity) with the results of microscopic SEM analyses,
(vi) Combine the results of resistivity imaging logs (especially dips and azimuths) with the results of core observations and the field samples from outcrops examination to establish proper location and geometry of fractures, faults and other observed discontinuities.

In our opinion, the novelty in fractured carbonates interpretation is using the machine deep learning techniques, and artificial intelligence to combine the super detailed data from X-ray computer tomography, and similar sophisticated laboratory technologies with continuous well logging measurements. Such approach generates costs, but gives hope for success, when petrophysicist are still faced with challenges of increased complication of geological conditions, when reaching for more and more difficult reservoirs. The fast development of computer aid technologies in many areas encourages us to apply them also in advanced petrophysics, and hopes to increase the effectiveness of research.

Author Contributions: Conceptualization: M.S. and J.A.J., methodology: M.S. and J.A.J., formal analysis: J.A.J., validation M.S., resources: M.S. and J.A.J., visualization: M.S., writing original draft: J.A.J., writing the corrections according to the reviewers: J.A.J. All authors have read and agreed to the published version of the manuscript.

Funding: This research didn't get an external funding.

Data Availability Statement: Data are not available.

Acknowledgments: The authors would like to express deep thanks to the Reviewers and Editors for their work.

Conflicts of Interest: The authors declare no conflict of interest.

References

1. Levorsen, A.I. *Geology of Petroleum*; W.H. Freeman & Company: San Francisco, CA, USA, 1965.
2. Tiab, D.; Donaldson, E.C. *Petrophysics: Theory and Practice of Measuring Reservoir Rock and Fluid Transport Properties*, 4th ed.; Gulf Professional Publishing, Elsevier: Oxford, UK, 2015.
3. Rothery, D. *Geology: A Complete Introduction*; Teach Yourself: London, UK, 2016; p. 384. ISBN 147360155X.
4. Rider, M.H. *Geological Interpretation of Well Logs*, 2nd ed.; Whittles Publishing: Dunbeath, UK, 1996.
5. Serra, O. *Well Logging Handbook*; Edition TECHNIP: Paris, France, 2008.

6. Chaudhry, A.U. Well Testing Methods for Naturally Fractured Reservoirs. In *Oil Well Testing Handbook*; Academic PR Inc.: Cambridge, MA, USA; Elsevier: Houston, TX, USA, 2004; 525p, ISBN 978-0750677066.
7. Wu, Y.-S. Multiphase Flow in Fractured Porous Media. In *Multiphase Fluid Flow in Porous and Fractured Reservoirs*; Imprint Gulf Professional Publishing, Elsevier Inc.: Amsterdam, The Netherlands, 2016; ISBN 978-0-12-803848-2. [CrossRef]
8. Palaz, I.; Marfurt, K.J. *Carbonate Seismology*; Geophysical Development Series; SEG: Tulsa, OK, USA, 1997.
9. Parra, R. Halliburton Basic Petroleum Geology and Log Analysis. 2001. Available online: https://www.academia.edu/6337349/1_Halliburton_Basic_Petroleum_geology_and_log_analysis (accessed on 15 December 2022).
10. Folk, R.L. Practical petrographic classification of limestones. *Bull. Am. Assoc. Pet. Geol.* **1959**, *43*, 1–38.
11. Folk, R.L. Spectral subdivision of limestone types. *AAPG Mem.* **1959**, *1*, 62–84.
12. Dunham, R.J. Classification of carbonate rocks according to depositional texture. *Mem. Am. Assoc. Pet. Geol.* **1962**, *1*, 108–121.
13. Wright, V.P. A revised classification of limestones. *Sediment. Geol.* **1992**, *76*, 177–185. [CrossRef]
14. Embry, A.F.; Klovan, J.E. A Late Devonian Reef Tract on Northeaster N Banks Island, N.W.T. *Bull. Can. Pet. Geol.* **1971**, *19*, 730–781.
15. Perras, M.A.; Diederichs, M.S. The importance of classification for carbonates and mudrocks in engineering. In Proceedings of the 2011 Pan-Am Canadian Geotechnical Conference, Toronto, ON, Canada, 1–7 October 2011.
16. Lokier, S.W.; Al Junaibi, M. The Petrographic Description of Carbonate Facies: Are We All Speaking the Same Language? *Sedimentology* **2016**, *63*, 7. [CrossRef]
17. Wagner, R.; Peryt, T.M. Possibility of sequence stratigraphic subdivision of the Zechstein in the Polish Basin. *Geol. Q.* **1997**, *41*, 457–474.
18. Jaworowski, K.; Mikołajewski, Z. Oil- and gas-bearing sediments of the Main Dolomite (Ca2) in the Międzychód region: A depositional model and the problem of the boundary between the second and third depositional sequences in the Polish Zechstein Basin. *Przegl. Geol.* **2007**, *55*, 1017–1024.
19. Leighton, M.W.; Pendexter, C. *Classification of Carbonate Rocks: A Symposium, Volume 1*; American Association of Petroleum Geologists: Tulsa, OK, USA, 1962.
20. Schön, J.H. *Physical Properties of Rocks: Fundamentals and Principles of Petrophysics*; Elsevier: Amsterdam, The Netherlands, 2015.
21. Hook, J.R. An introduction to porosity. *Petrophysics* **2003**, *44*, 205–212.
22. Valentín, M.B.; Bom, C.R.; Compan, A.L.M.; Correia, M.D.; Menezes de Jesus, C.; de Lima Souza, A.; de Albuquerque, M.P.; de Albuquerque, M.P.; Faria, E.L. Estimation of permeability and effective porosity logs using deep autoencoders in borehole image logs from the Brazilian pre-salt carbonate. *J. Pet. Sci. Eng.* **2018**, *170*, 315–330. [CrossRef]
23. Guo, J.C.; Zhao, Z.H.; He, S.G.; Liang, H.; Liu, Y.X. A new method for shale brittleness evaluation. *Environ. Earth Sci.* **2015**, *73*, 5855–5865. [CrossRef]
24. Jarvie, D.M.; Hill, R.J.; Ruble, T.E.; Pollastro, R.M. Unconventional shale-gas systems: The Mississippian Barnett Shale of northcentral Texas as one model for thermogenic shale-gas assessment. *AAPG Bull.* **2007**, *91*, 475–499. [CrossRef]
25. Meng, F.; Wong, L.N.Y.; Zhou, H. Rock brittleness indices and their applications to different fields of rock engineering: A review. *J. Rocks Mech. Geotech. Eng.* **2021**, *13*, 221–247. [CrossRef]
26. Cleary, M.P. Theory and Application of Hydraulic Fracturing technology. In *Hydraulic Fracturing and Geothermal Energy*; Springer: Berlin/Heidelberg, Germany, 1983; pp. 267–289.
27. Asgarinezhad, Y.; Asgarinezhad, M.; Tokhmechi, B.; Kamkar-Rouhani, A.; Sherkati, S. Detecting vuggy porosity in carbonate reservoirs by well logs. *J. Pet. Explor. Prod. Technol.* **2016**, *6*, 25–31. [CrossRef]
28. Akram, A.H.; Gherryo, Y.S.; Ali, S.M.; Thabt, M.S.; Serban, A. Dynamic behavior of a fissured dual-carbonate reservoir modeled with DFN. In Proceedings of the SPE North Africa Technical Conference and Exhibition, Cairo, Egypt, 14–17 February 2010.
29. Gomaa, N.; Al-Alyak, A.; Ouzzane, D.; Saif, O.; Okuyiga, M.; Allen, D.; Rose, D.; Ramamoorthy, R.; Bize, E. Case study of permeability, vug quantification, and rock typing in a complex carbonate. In Proceedings of the SPE Annual Technical Conference and Exhibition, San Antonio, TX, USA, 24–27 September 2006.
30. Available online: https://glossary.slb.com (accessed on 5 December 2022).
31. KGS, Oil and Gas Reports. *The Role of Moldic Porosity in Paleozoic Kansas Reservoirs and the Association of Original Depositional Facies and Early Diagenesis with Reservoir Properties*; Open File Report 2003-32; Kansas Geological Survey: Lawrence, KS, USA, 12 May 2023.
32. Amour, F.; Nick, H.M. Porosity and permeability variability across a chalk reservoir in the Danish North Sea: Quantitative impacts of depositional and diagenetic processes. *Eng. Geol.* **2021**, *285*, 106059. [CrossRef]
33. Fabricius, I.L. Chalk composition, Diagenesis and physical properties. *Geol. Soc. Den. Bull.* **2007**, *55*, 97–128. [CrossRef]
34. Agarwal, B.; Aalen, L.R.; Farrell, H.E. Ekofisk Field Reservoir Characterization: Mapping Permeability Through Facies and Fracture Intensity. *SPE Form. Eval.* **1997**, *12*, 227–233. [CrossRef]
35. Powley, D.E. Pressures and hydrogeology in petroleum basins. *Earth Sci. Rev.* **1990**, *29*, 215–226.
36. Zhang, J. Pore pressure prediction from well logs: Methods, modifications, and new approaches. *Earth-Sci. Rev.* **2011**, *108*, 1–2. [CrossRef]
37. Darcy, H. Les Fontaines Publiques de la Ville de Dijon: Exposition et Application des Principes à Suivre et des Formules à Employer Dans Les Questions De Distribution d'eau: OUVRAGE Terminé par un Appendice Relatif aux Fournitures d'eau de Plusieurs Villes, au Filtrage des Eaux et à la Fabrication des Tuyaux de Fonte, de Plomb, de Tôle et de Bitumen. Victor Dalmont. 1856. Available online: https://gallica.bnf.fr/ark:/12148/bpt6k624312/f1n657.pdf (accessed on 5 December 2022).

38. Honarpour, M.; Koederitz, L.; Harvey, A.H. *Relative Permeability of Petroleum Reservoirs*; CRC Press: Boca Raton, FL, USA, 2018.
39. Lucia, F.J. Petrophysical parameters estimated from visual description of carbonate rocks: A field classification of carbonate pore space. *J. Pet. Technol.* **1983**, *35*, 626–637. [CrossRef]
40. Lucia, F.J. Carbonate Reservoir Models: Facies, Diagenesis, and Flow Characterization. In *Development Geology Reference Manual*; Morton-Thompson, D., Woods, A.M., Eds.; AAPG: Tulsa, OK, USA, 1993; Volume 10, pp. 269–274.
41. Lucia, F.J. Rock-Fabric/Petrophysical Classification of Carbonate Pore Space for Reservoir Characterization. *AAPG Bull.* **1995**, *79*, 1275–1300.
42. Lucia, F.J. *Carbonate Reservoir Characterization: An Integrated Approach*; Springer: Berlin/Heidelberg, Germany, 2007; p. 336.
43. Lucia, F.J.; Conti, R.D. *Rock Fabric, Permeability, and Log Relationships in an Upward-Shoaling, Vuggy Carbonate Sequence*; University of Texas at Austin, Bureau of Economic Geology: Austin, TX, USA, 1987.
44. Lucia, F.J.; Kerans, C.; Senger, R.K. Defining flow units in dolomitized carbonate-ramp reservoirs. In Proceedings of the SPE Annual Technical Conference and Exhibition, Washington, DC, USA, 4–7 October 1992; pp. 399–406.
45. Archie, G.E. Classification of Carbonate Reservoir Rocks and Petrophysical Considerations. *Bull. Am. Assoc. Pet. Geol.* **1952**, *36*, 278–298.
46. Ehrenberg, S.N.; Eberli, G.P.; Keramati, M.; Moallemi, S.A. Porosity-permeability relationships in interlayered limestone-dolostone reservoirs. *AAPG Bull.* **2006**, *90*, 91–114. [CrossRef]
47. Hull, C.E.; Warman, H.R. Asmari oil fields of Iran. In *Geology of Giant Petroleum Fields*; Halbouty, M.T., Ed.; AAPG: Tulsa, OK, USA, 1989; Volume 14, pp. 428–437.
48. McQuillan, H. Fracture-controlled production from the Oligo-Miocene Asmari Formation in Gachsaran and Bibi Hakimeh fields, southwest Iran. In *Carbonate Petroleum Reservoirs*; Roehl, P.O., Choquette, P.W., Eds.; Springer: New York, NY, USA, 2001.
49. Crockett, J. Porosity Evolution of the Madison Limestone, Mississippian: Wind River Basin, Wyoming. Master's Thesis, Louisiana State University, Baton Rouge, LA, USA, 1994.
50. Sonnenfeld, M.D. Sequence Evolution and Hierarchy within the Lower Mississippian Madison Limestone of Wyoming. In *Paleozoic Systems of the Rocky Mountain Region: Rocky Mountain Section*; Longman, M.W., Sonnenfeld, M.D., Eds.; Society of Economic Paleontologists and Mineralogists: Washington, DC, USA, 1996; pp. 165–192.
51. Ehrenberg, S.N. Factors controlling porosity in Upper Carboniferous–Lower Permian carbonate strata of the Barents Sea. *AAPG Bull.* **2004**, *88*, 1653–1676. [CrossRef]
52. Melim, L.A.; Anselmetti, F.S.; Eberli, G.P. The importance of pore type on permeability of Neogene carbonates, Great Bahama Bank. In *Subsurface Geology of a Prograding Carbonate Platform Margin, Great Bahama Bank: Results of the Bahamas Drilling Project: SEPM Special Publication*; Ginsburg, R.N., Ed.; Society of Economic Paleontologists and Mineralogists: Washington, DC, USA, 2001; Volume 70, pp. 217–238.
53. Isern, A.R. *Proceedings of the Ocean Drilling Program, Initial Reports: Ocean Drilling Program*; Texas A&M University: College Station, TX, USA, 2002; Volume 194, p. 88.
54. Smith, L.B., Jr.; Eberli, G.P.; Sonnenfeld, M. Sequence stratigraphic and paleogeographic distribution of reservoir quality dolomite, Madison Formation, Wyoming and Montana. In *Integration of Outcrop and Modern Analogs in Reservoir Modeling*; AAPG: Tulsa, OK, USA, 2004; pp. 67–92.
55. Westphal, H.; Eberli, G.P.; Smith, L.B.; Grammer, G.M.; Kislak, J. Reservoir characterization of the Mississippian Madison Formation, Wind River basin, Wyoming. *AAPG Bull.* **2004**, *88*, 405–432. [CrossRef]
56. Heffer, K. Fracture characterization through rate correlation analysis. In Proceedings of the EAGE Annual Conference & Exhibition Incorporating SPE Europec 2012, Copenhagen, Denmark, 4–7 June 2012.
57. Hensel, W.M., Jr. A Perspective Look at Fracture Porosity. *SPE Form. Eval.* **1989**, *4*, 531–534. [CrossRef]
58. Reiss, L.H. *The Reservoir Engineering Aspects of Fractured Formations*; Gulf Publishing Co.: Houston, TX, USA, 1980.
59. Stadtműller, M. Well logging interpretation methodology for carbonate formation fracture system properties determination. *Acta Geophys.* **2019**, *67*, 1933–1943. [CrossRef]
60. Paduszyński, J. Szacowanie gęstości mikroszczelin metodą trawersów losowych. *Nafta* **1965**, *1*, 2–3.
61. Gamal, M.; El-Araby, A.A.; El-Barkooky, A.N.; Hassan, A. Detection and characterization of fractures in the Eocene Thebes formation using conventional well logs in October field, Gulf of Suez, Egypt. *Egypt. J. Pet.* **2022**, *31*, 1–9. [CrossRef]
62. Advanced Borehole Imaging Independent of Mud Type, SMP-5871. 2002. Available online: www.connect.slb.com (accessed on 5 December 2022).
63. Available online: https://hesp.com/index.php/services/open-hole/imaging/cast-i-circumferential-acoustic-scanning-tool-logiq (accessed on 16 February 2023).
64. Deltombe, J.-L.; Schepers, R. Combined processing of BHTV travel time and amplitude images. In Proceedings of the 7th International Symposium on Minerals and Geotechnical Logging, Golden, CO, USA, 24–26 October 2000.
65. Lai, J.; Wang, G.; Fan, Z.; Wang, Z.; Chen, J.; Zhou, Z.; Wang, S.; Xiao, C. Fracture detection in oil-based drilling mud using a combination of borehole image and sonic logs. *Marine Petrol. Geol.* **2017**, *84*, 195–214. [CrossRef]
66. Ekstrom, M.P.; Dahan, C.A.; Chen, D.Y.; Lloyd, P.M.; Rossi, D.J. Formation imaging with microelectrical scanning arrays. *Log Anal.* **1987**, *28*, 295–306.
67. Tingay, M.; Reinecker, J.; Műller, B. Borehole Breakout and Drilling-Induced Fracture Analysis from Image Logs. World Stress Map Project. Guidelines: Image Logs. Available online: www.world-stress-map.org (accessed on 13 January 2023).

68. Sowiżdżał, K.; Stadtműller, M. Metodyka konstrukcji przestrzennych modeli szczelinowatości poziomów zbiornikowych. *Nafta-Gaz* **2010**, *3*, 159–166. (In Polish)
69. Jarzyna, J.A.; Baudzis, S.; Janowski, M.; Puskarczyk, E. Geothermal Resources Recognition and Characterization on the Basis of Well Logging and Petrophysical Laboratory Data, Polish Case Studie. *Energies* **2021**, *14*, 850. [CrossRef]
70. Available online: https://wiki.aapg.org/Dipmeter (accessed on 13 January 2023).
71. Ciuperca, C.; Badulescu, C.; Niculescu, B.; Negut, A. Identification of Open Natural Fractures using Conventional Wireline Logs, Borehole Imaging and Stoneley Waves. In Proceedings of the 9th Congress of the Balkan Geophysical Society, Antalya, Turkey, 5–9 November 2017.
72. Hornby, B.E.; Johnson, D.L.; Winkler, K.W.; Plumb, R.A. Fracture evaluation using reflected Stoneley-wave arrivals. *Geophysics* **1989**, *54*, 1274–1288. [CrossRef]
73. Cheng, C.H.; Paillet, F.L.; Pennington, W.D. Acoustic Waveform Logging—Advances in Theory and Application. *Log Anal.* **1992**, *33*, SPWLA-1992-v33n3a2.
74. Haldorsen, J.B.U.; Johnson, D.J.; Plona, T.; Sinha, B.; Valero, H.-P.; Winkler, K. Borehole acoustic waves. *Oilfield Rev.* **2006**, *18*, 34–43.
75. Cassel, B.; Badri, M.; Faulhaber, J. Permeability prediction based on anelastic attenuation using Dipole Shear and Low Frequency monopole sources in a Carbonate Reservoir in Saudi Arabia. In Proceedings of the GEO-94 Middle East Geosciences Exhibition & Conference, Manama, Bahrain, 25–27 April 1994.
76. Rajabi, A.; Moein, M.J.A.; Rabbani, A.R. Improvement of petrophysical evaluation in a gas bearing carbonate reservoir. A case in Persian Gulf. *J. Nat. Gas Sci. Eng.* **2015**, *24*, 238–244. [CrossRef]
77. Akbar, M.; Petricola, M.; Watfa, M.; Badri, M.; Charara, M.; Boyd, A.; Cassel, B.; Nurmi, R.; Delhomme, J.-P.; Grace, M.; et al. Classic Interpretation Problems: Evaluating Carbonates. *Oilfield Rev.* **1995**, *7*, 38–57.
78. Coates, G.R.; Xiao, L.; Prammer, M.G. *NMR logging Principles & Applications*; Halliburton Energy Services: Houston, TX, USA, 1999.
79. Jarzyna, J.A.; Maziarka, D.; Pasek, P.; Klaja, J.; Krakowska, P.; Puskarczyk, E. Results of MRIL well logging and NMR laboratory experiments for reservoir rocks evaluation. *Przegl. Geol.* **2017**, *65*, 109–121. Available online: https://www.pgi.gov.pl/dokumenty-pig-pib-all/publikacje-2/przeglad-geologiczny/2017 (accessed on 5 December 2022).
80. Mahiout, S.; Clerke, E.A.; Belowi, A.; Qubaisi, K.; Qatari, A. Complex Gas Bearing Carbonate Reservoir Evaluation—A Case Study from Saudi Arabia. In Proceedings of the SPWLA 55th Annual Logging Symposium, Abu Dhabi, United Arab Emirates, 18–22 May 2014.
81. Al Shehhi, N.; El-Hamawi, M.; Al Arfi, S.; Desport, O.; Padiav, P. Petrophysical Evaluation of a Gas Carbonates Reservoir through Integrated Workflow. In Proceedings of the Abu Dhabi International Petroleum Conference and Exhibition, Abu Dhabi, United Arab Emirates, 11–14 November 2012.
82. Ramakrishnan, T.S.; Ramamoorthy, R.; Fordham, E.; Schwartz, L.; Herron, M.; Saito, N.; Ramamoorthy, R.; Boyd, A.; Neville, T.J.; Seleznev, N.; et al. A New Workflow for Petrophysical and Textural Evaluation of Carbonate Reservoirs. In Proceedings of the SPWLA 49th Annual Logging Symposium, Austin, TX, USA, 25–28 May 2008.
83. Ghoochaninejad, H.Z.; Asef, M.R.; Moallemi, S.A. Estimation of fracture aperture from petrophysical logs using teaching–learning-based optimization algorithm into a fuzzy inference system. *J. Pet. Explor. Prod. Technol.* **2018**, *8*, 143–154. [CrossRef]
84. Luthi, S.M.; Souhaite, P. Fracture apertures from electrical borehole scans. *J. Geophys.* **1990**, *55*, 821–833. [CrossRef]
85. Faivre, O. Fracture evaluation from quantitative azimuthal resistivity. In Proceedings of the SPE Annual Technical Conference and Exhibition, Houston, TX, USA, 3–6 October 1993; pp. 179–192.
86. Ranjith, P.G.; Viete, D.R. Applicability of the 'cubic law' for non-Darcian fracture flow. *J. Pet. Sci. Eng.* **2011**, *78*, 321–327. [CrossRef]
87. Watanabe, N.; Hirano, N.; Tsuchiya, N. Determination of aperture structure and fluid flow in a rock fracture by high-resolution numerical modeling on the basis of a flow-through experiment under confining pressure. *Water Resour. Res.* **2008**, *44*. [CrossRef]
88. Wellington, S.L.; Vinegar, H. X-ray computerized tomography. *J. Pet. Technol.* **1987**, *9*, 885–898. [CrossRef]
89. Montemagno, C.D.; Pyrak-Nolte, L.J. Fracture network versus single fractures: Measurement of fracture geometry with X-ray tomography. *Phys. Chem. Earth Part A* **1999**, *24*, 575–577. [CrossRef]
90. Bertels, S.P.; DiCarlo, D.A.; Blunt, M.J. Measurement of aperture distribution, capillary pressure, relative permeability, and in situ saturation in a rock fracture using computed tomography scanning. *Water Resour. Res.* **2001**, *37*, 649–662. [CrossRef]
91. Stadtműller, M.; Krakowska-Madejska, P.I.; Leśniak, G.; Jarzyna, J.A. Characterization of the Carbonate Formation Fracture System Based on Well Logging Data and Results of Laboratory Measurements. *Energies* **2021**, *14*, 6034. [CrossRef]
92. Krakowska-Madejska, P.I. New filtration parameters from X-ray computed tomography for tight rock images. *Geol. Geophys. Environ.* **2022**, *48*, 381–392. [CrossRef]
93. Yu, X.; Butler, S.K.; Kong, L.; Mibeck, B.A.F.; Barajas-Olalde, C.; Burton-Kelly, M.E.; Azzolina, N.A. Machine learning-assisted upscaling analysis of reservoir rock core properties based on micro-computed tomography imagery. *J. Pet. Sci. Eng.* **2022**, *219*, 11108. [CrossRef]
94. Tsakiroglu, C.D.; Payatakes, A.C. Characterization of the pore structure of reservoir rocks with the aid of serial sectioning analysis, mercury porosimetry and network simulation. *Adv. Water Resour.* **2000**, *23*, 773–789. [CrossRef]

95. Karpyn, Z.T.; Alajmi, A.; Radaelli, F.; Halleck, P.M.; Grader, A.S. X-ray CT and hydraulic evidence for a relationship between fracture conductivity and adjacent matrix porosity. *Eng. Geol.* **2009**, *103*, 139–145. [CrossRef]
96. Ja'fari, A.; Kadkhodaie-Ilkhchi, A.; Sharghi, Y.; Ghanavati, K. Fracture density estimation from petrophysical log data using the adaptive neuro-fuzzy inference system. *J. Geophys. Eng.* **2012**, *9*, 105–114. [CrossRef]
97. Chiu, S. Fuzzy model identification based on cluster estimation. *J. Intell. Fuzzy Syst.* **1994**, *2*, 267–278. [CrossRef]
98. Zadeh, L.A. Fuzzy sets. *Inf. Control* **1965**, *8*, 338–353. [CrossRef]
99. Rostami, A.; Kordavani, A.; Parchekhari, S.; Hemmati-Sarapardeh, A.; Helalizadeh, A. New insights into permeability determination by coupling Stoneley wave propagation and conventional petrophysical logs in carbonate oil reservoirs. *Sci. Rep.* **2022**, *12*, 11618. [CrossRef]
100. Da Silva, E.Y. Primary and Enhanced Recovery of Ekofisk Field. A Single-and Double-Porosity Numerical Simulation Study. In Proceedings of the SPE Annual Technical Conference and Exhibition, San Antonio, TX, USA, 8–11 October 1989.
101. Thomas, L.K.; Dixon, T.N.; Pierson, R.G. Ekofisk Nitrogen Injection. In Proceedings of the SPE Annual Technical Conference and Exhibition, San Antonio, TX, USA, 8–11 October 1989; pp. 151–160. [CrossRef]
102. Stadtműller, M.; Kowalik, J. Possibilities of Fracture Aperture Evaluation Based on Well Logs-Methodical Aspects. In Proceedings of the GEOPETROL 2012 Conference, Zakopane, Poland, 29 September 2012; pp. 355–358.
103. Ramamoorthy, R.; Ramakrishnan, T.S.; Dasgupta, S.; Raina, I. Towards a Petrophysically Consistent Implementation of Archie's Equation for Heterogeneous Carbonate Rocks. *Petrophysics* **2020**, *61*, 450–472. [CrossRef]
104. Petricola, M.J.C.; Takezaki, H.; Asakura, S. Saturation Evaluation in Micritic Reservoirs: Raising to the Challenge. In Proceedings of the Abu Dhabi International Petroleum Exhibition and Conference 2012, Abu Dhabi, United Arab Emirates, 13–16 October 2012. [CrossRef]
105. Ramakrishnan, T.S.; Rabaute, A.; Fordham, E.J.; Ramamoorthy, R.; Herron, M.; Matteson, A.; Raghuraman, B.; Mahdi, A.; Akbar, M.; Kuchuk, F. A Petrophysical and Petrographic Study of Carbonate Cores From the Thamama Formation. In Proceedings of the 8th Abu Dhabi International Petroleum Exhibition and Conference, Abu Dhabi, United Arab Emirates, 11–14 October 1998. [CrossRef]
106. Ramakrishnan, T.S.; Ramamoorthy, R.; Fordham, E.; Schwartz, L.; Herron, M.; Saito, N.; Rabaute, A. A Model Based Interpretation Methodology for Evaluating Carbonate Reservoirs. In Proceedings of the SPE Annual Technical Conference and Exhibition 2001, New Orleans, LA, USA, 30 September–3 October 2001. [CrossRef]
107. Skalinski, M.; Kenter, J.A.M. Carbonate Petrophysical Rock Typing: Integrating Geological Attributes and Petrophysical Properties While Linking with Dynamic Behaviour. 2014. Available online: http://sp.lyellcollection.org/ (accessed on 20 February 2023).
108. Gianotten, I.P.; Rameil, N.; Foyn, S.E.; Kollien, T.; Marre, J.R.; Looyestijn, W.; Zhang, X.; Hebing, A. Free or Bound? Thomeer and NMR Porosity Partitioning in Carbonate Reservoirs, Alta Discovery, Southwestern Barents Sea. *Petrophysics* **2021**, *62*, 175–194. [CrossRef]
109. Krogulec, E.; Sawicka, K.; Zabłocki, S.; Falkowska, E. Mineralogy and Permeability of Gas and Oil Dolomite Reservoirs of the Zechstein Main Dolomite Basin in the Lubiatów Deposit (Poland). *Energies* **2020**, *13*, 6436. [CrossRef]
110. Bohnsack, D.; Potten, M.; Pfrang, D.; Wolpert, P.; Zosseder, K. Porosity–permeability relationship derived from Upper Jurassic carbonate rock cores to assess the regional hydraulic matrix properties of the Malm reservoir in the South German Molasse Basin. *Geotherm. Energy* **2020**, *8*, 2–47. [CrossRef]
111. Rashid, F.; Glover, P.W.J.; Lorinczi, P.; Collie, R.; Lawrence, J. Porosity and permeability of tight carbonate reservoir rocks in the north of Iraq. *J. Pet. Sci. Eng.* **2015**, *133*, 147–161. [CrossRef]
112. Maniscalco, R.; Fazio, E.; Punturo, R.; Cirrincione, R.; Di Stefano, A.; Distefano, S.; Forzese, M.; Lanzafame, G.; Leonardi, G.S.; Montalbano, S.; et al. The Porosity in Heterogeneous Carbonate Reservoir Rocks: Tectonic versus Diagenetic Imprint—A Multi-Scale Study from the Hyblean Plateau (SE Sicily, Italy). *Geosciences* **2022**, *12*, 149. [CrossRef]
113. Amer Attique, M.; Ehsan, M.; Akhtar Javid, M. Significance of real-time petro-physical data for an optimal remote geosteering operation in complex geological reservoirs. *Geol. Geophys. Environ.* **2021**, *47*, 125–130. [CrossRef]
114. Kubik, B.; Kowalska, S.; Skupio, R.; Zagórska, U.; Wolański, K. Possibilities of using lithological profiles prepared on the basis of the results of chemical composition measurements using the pXRF method on core and aggregate samples. *Wiadomości* **2020**, *2*, 256.